JACS
JOURNAL OF THE AMERICAN CHEMICAL SOCIETY

# Redox Switchable Daisy Chain Rotaxanes Driven by Radical-Radical Interactions

Carson J. Bruns,[†] Marco Frasconi,[†] Julien Iehl,[†] Karel J. Hartlieb,[†] Severin T. Schneebeli,[†] Chuyang Cheng,[†] Samuel I. Stupp,[†,‡,§]* J. Fraser Stoddart[†]*

[†]Department of Chemistry
[‡]Department of Materials Science and Engineering
[§]Department of Medicine

*Northwestern University, 2145 Sheridan Road, Evanston, Illinois, 60208 (USA)*

## SUPPORTING INFORMATION

**Table of Contents**

## 1. General Methods

All reagents and solvents were purchased from Sigma-Aldrich and used without further purification. The following compounds – 4,7-dimethylisoindoline-1,3-dione,[S1] **HS**$^{2+}$,[S2] **BHEEN**,[S3] **BN$_3$EEEN**,[S4] **HV**·2PF$_6$,[S5] and the stopper precursor **St**[S6] – were prepared according to literature procedures. All reactions were performed under a nitrogen atmosphere unless otherwise stated. Thin layer chromatography (TLC) was performed on silica gel 60 $F_{254}$ (E. Merck) and visualized under a UV lamp at 254 nm. Column chromatography was carried out on silica gel 60 (Sorbent Technologies, 40–63 mm. A C-18 column was used for analytical and preparative reverse phase high performance liquid chromatography (RP-HPLC) on Shimadzu Prominence LC-20 and Shimadzu Prominence LC-8a instruments, respectively, eluting with $H_2O$/MeCN (0.1 % v/v TFA) and monitored using a UV detector ($\lambda$ = 254 nm). UV/Vis Spectra were recorded at room temperature on a Shimadzu UV-3600 spectrophotometer. Nuclear magnetic resonance (NMR) spectra were recorded on Bruker Avance 500 and 600 spectrometers with working frequencies of 500 and 600 MHz for $^1$H, and 125 and 150 MHz for $^{13}$C nuclei, respectively. Chemical shifts are reported in ppm and referenced to the residual non-deuterated solvents for $^1$H ($CDCl_3$: $\delta$ = 7.27 ppm, $CD_3CN$: $\delta$ = 1.94 ppm) and $^{13}$C ($CDCl_3$: $\delta$ = 77.0 ppm, $CD_3CN$: $\delta$ = 118.26 ppm). High-resolution mass spectra (HRMS) were measured in electrospray ionization (ESI) mode on an Agilent 6210 LC-TOF mass spectrometer with sample introduction via an Agilent 1200 HPLC. Cyclic voltammetry (CV) experiments were carried out at room temperature in argon-purged solutions of MeCN with a Gamry Multipurpose instrument interfaced to a PC. CV Experiments were performed using a glassy carbon working electrode (0.071 cm$^2$, Cypress system), and the electrode surface was polished routinely with 0.05 μm alumina-water slurry on a felt surface immediately before use. The counter electrode was a Pt coil and the reference electrode a saturated calomel electrode. Experimental errors are within potential values of ± 10 mV. Spectroelectrochemistry (SEC) experiments were carried out using a custom-built optically transparent thin-layer electrochemical cell with an optical path of 2 mm using a Pt grid as working electrode, a Pt wire counter electrode, and a Ag wire pseudo-reference electrode.

## 2. Synthetic Procedures

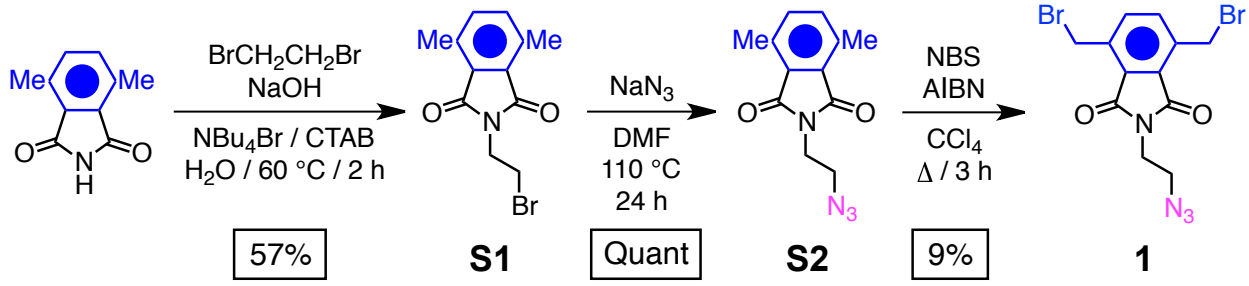


**Scheme S1.** Synthesis of compound **1**

**S1**. A 10 M aqueous solution (2.5 mL) of NaOH was added with stirring to a suspension of 4,7-dimethylisoindoline-1,3-dione (3.3 g, 19 mmol), tetrabutylammonium bromide (200 mg, 0.6 mmol), and cetyltrimethylammonium bromide (200 mg, 0.5 mmol) in 1,2-dibromoethane (16 g, 85 mmol) and the mixture was heated at 60 °C for 2 h. The reaction mixture was extracted with $CH_2Cl_2$ (3 × 20 mL) in $H_2O$ (40 mL). The organic extracts were combined, dried ($MgSO_4$), filtered, concentrated, and subjected to flash column chromatography on $SiO_2$ in $CH_2Cl_2$ to afford the product as a white solid (3.0 g, 57%). $^1$H NMR (500 MHz, $CDCl_3$, 298 K) $\delta$ = 7.34 (s, 2H), 4.08 (t, $J$ = 6.7 Hz, 2H), 3.61 (t, $J$ = 6.7 Hz, 2H), 2.66 (s, 6H). $^{13}$C NMR (125 MHz, $CDCl_3$, 298 K) $\delta$ = 168.6, 136.3, 135.6, 128.6, 38.9, 28.4, 17.4. HRMS (ESI-TOF-MS): *m/z* calcd for $C_{12}H_{13}BrNO_2$ $[M + H]^+$ 282.0125, observed 282.0123.

**S2**. A mixture of sodium azide (2.0 g, 31 mmol) and **S1** (3.0 g, 11 mmol) in DMF (15 mL) was heated at 90 °C for 24 h. The solvent was removed under vacuum and the residue was partitioned between $CH_2Cl_2$ (20 mL) and $H_2O$ (40 mL). The aqueous layer was extracted with $CH_2Cl_2$ (3 × 20 mL) and the extracts were combined, dried ($MgSO_4$), and filtered. After removal of the solvent, the product **S2** was obtained as a white solid (2.6 g, 100%). $^1$H NMR (500 MHz, $CDCl_3$, 298 K) $\delta$ = 7.34 (s, 2H), 3.86 (t, $J$ = 6.1 Hz, 2H), 3.59 (t, $J$ = 6.1 Hz, 2H), 2.66 (s, 6H). $^{13}$C NMR (125 MHz, $CDCl_3$, 298 K) $\delta$ = 168.8, 136.2, 135.6, 128.6, 49.1, 36.4, 17.4. HRMS (ESI-TOF-MS): *m/z* calcd for $C_{12}H_{12}N_4NaO_2$ $[M + Na]^+$ 267.0853, observed 267.0864.

**1**. A mixture of **S2** (2.48 g, 10.1 mmol), *N*-bromosuccinimide (3.43 g, 19.3 mmol), and azobisisobutyronitrile (100 mg, 0.61 mmol) in $CCl_4$ (90 mL) was heated under reflux for 3 h.

The crude mixture was filtered and the filtrate was concentrated and purified by flash column chromatography on $SiO_2$ (8:1:1 hexanes:$CH_2Cl_2$:EtOAc) to afford the product **1** as a white solid (283 mg, 9%). $^1$H NMR (500 MHz, $CDCl_3$, 298 K) $\delta$ = 7.73 (s, 2H), 4.97 (s, 2H), 3.90 (t, $J$ = 6.2 Hz, 2H), 3.62 (t, $J$ = 6.2 Hz, 2H). $^{13}$C NMR (125 MHz, $CDCl_3$, 298 K) $\delta$ = 167.1, 137.1, 136.6, 128.3, 48.8, 36.9, 25.7. HRMS (ESI-TOF-MS): *m/z* calcd for $C_{12}H_{10}Br_2N_4NaO_2$ $[M + Na]^+$ 422.9063, observed 422.9068.

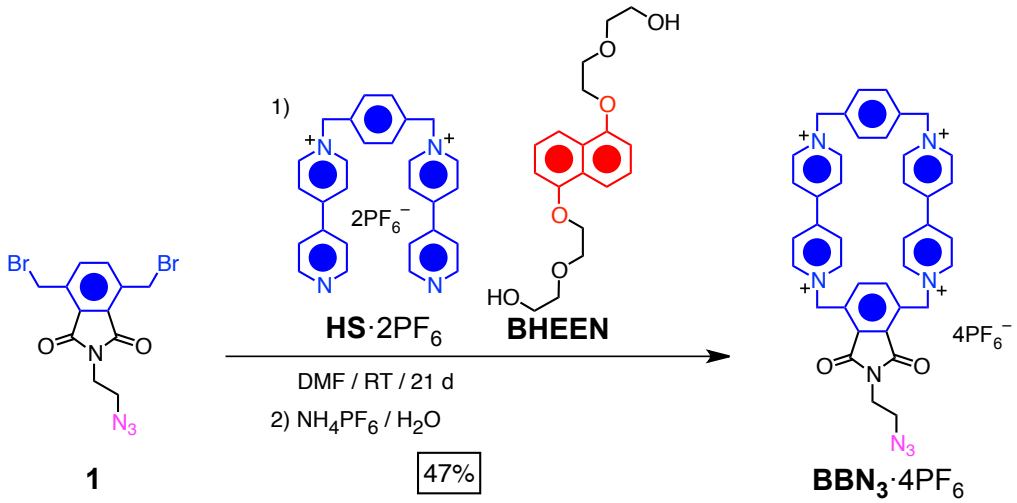


**Scheme S2**. Synthesis of symmetrical azide blue box **BBN$_3$**·4$PF_6$

**BBN$_3$**$^{4+}$. A mixture of **1** (250 mg, 0.62 mmol), **HS**·2$PF_6$ (450 mg, 0.64 mmol), and **BHEEN** (1.1 g, 3.3 mmol) in DMF (25 mL) was stirred at ambient temperature for 28 d. The mixture was filtered and concentrated to a volume of 10 mL. The charged products were precipitated by the addition of $NBu_4Br$ (2 g), diluted with $CH_2Cl_2$ (50 mL), and collected by vacuum filtration. The collected solids were combined and dissolved in $H_2O$ (50 mL) and subjected to continuous liquid-liquid extraction in $CHCl_3$ overnight, during which time the aqueous layer changed color from red to yellow. The aqueous layer was concentrated to approximately 5 mL and filtered before being purified by preparative HPLC, eluting with $H_2O$/MeCN (0–40% MeCN in 40 min). Pure fractions were verified by analytical HPLC, combined, concentrated, and added to a saturated solution of aqueous $NH_4PF_6$ (5 mL) to afford **BBN$_3$**·4$PF_6$ as a white precipitate (365 mg, 47%). $^1$H NMR (500 MHz, $CD_3CN$, 298 K) $\delta$ = 8.91 (d, $J$ = 7.0 Hz, 4H), 8.90 (d, $J$ = 7.0 Hz, 4H), 8.21 (d, $J$ = 7.0 Hz, 4H), 8.14 (d, $J$ = 7.0 Hz, 4H), 8.10 (s, 2H), 7.50 (s, 4H), 6.20 (s, 4H), 5.77 (s, 4H), 3.74 (t, $J$ = 5.9 Hz, 2H), 3.55 (t, $J$ = 5.9 Hz, 2H). $^{13}$C NMR (125 MHz, $CD_3CN$, 298 K) $\delta$ = 168.3, 150.7, 150.6, 146.9, 146.0, 138.3, 136.9, 133.9, 131.6, 131.0, 128.4, 127.8, 65.5,

60.1, 49.4, 38.1. HRMS (ESI-TOF-MS): *m/z* calcd for $C_{40}H_{34}F_{18}N_8O_2P_3$ $[M - PF_6]^+$ 1093.1725, observed 1093.1759; *m/z* calcd for $C_{40}H_{34}F_{12}N_8O_2P_2$ $[M - 2PF_6]^{2+}$ 474.1039, observed 474.1058.

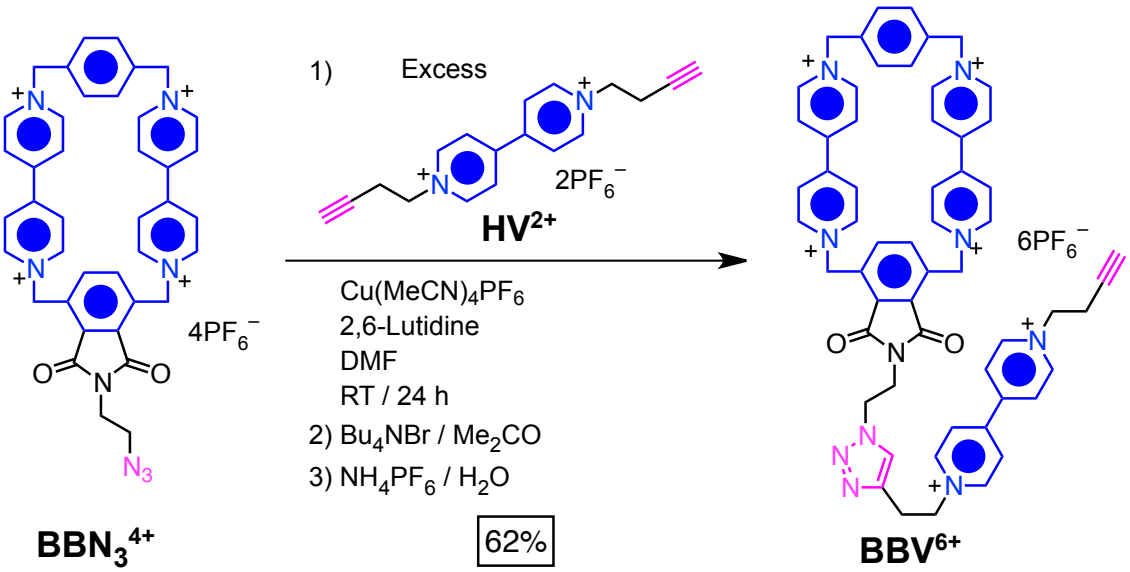


**Scheme S3**. Synthesis of blue box–viologen compound **BBV**·6$PF_6$

**BBV·6PF$_6$**. Compound **BBN$_3$**·4$PF_6$ (200 mg, 0.16 mmol) was added to a degassed solution of **HV**·2$PF_6$ (500 mg, 0.91 mmol) in DMF (3 mL). $Cu(MeCN)_4PF_6$ (25 mg, 0.067 mmol) and 2,6-lutidine (10 μL) were each added in one portion and the reaction mixture stirred at ambient temperature for 24 h. The solvent was removed under vacuum and the residue was dissolved in $Me_2CO$ (1 mL). The positively charged product was precipitated by the addition of a solution of $Bu_4NBr$ (500 mg) in $Me_2CO$ (2 mL). The precipitate was collected by centrifugation, dissolved in $H_2O$ (5 mL), and purified by preparative HPLC, eluting with $H_2O$/MeCN (0–40% MeCN in 40 min). Pure fractions were verified by analytical HPLC, combined, concentrated, and added to a saturated aqueous solution of $NH_4PF_6$ (5 mL) to afford **BBV**·6$PF_6$ as a white precipitate. (180 mg, 62%). $^1$H NMR (500 MHz, $CD_3CN$, 298 K) $\delta$ = 8.95 (d, $J$ = 7.0 Hz, 2H), 8.88 (d, $J$ = 7.0 Hz, 2H), 8.87 (d, $J$ = 7.1 Hz, 4H), 8.84 (d, $J$ = 6.6 Hz, 4H), 8.43 (d, $J$ = 7.0 Hz, 2H), 8.40 (d, $J$ = 7.0 Hz, 2H), 8.21 (d, $J$ = 6.6 Hz, 4H), 8.16 (d, $J$ = 7.1 Hz, 4H), 8.04 (s, 2H), 7.67 (s, 1H), 7.48 (s, 4H), 6.14 (s, 4H), 5.74 (s, 4H), 4.97 (t, $J$ = 7.0 Hz, 2H), 4.77 (t, $J$ = 6.4 Hz, 2H), 4.54 (t, $J$ = 5.8 Hz, 2H), 3.92 (t, $J$ = 5.8 Hz, 2H), 3.47 (t, $J$ = 7.0 Hz, 2H), 2.98 (td, $J$ = 2.6, 6.4 Hz, 2H), 2.46 (t, $J$ = 2.6 Hz, 1H). $^{13}$C NMR (125 MHz, $CD_3CN$, 298 K) $\delta$ = 168.1, 150.6, 151.3, 151.0, 150.5, 146.8, 146.7, 146.7, 146.0, 142.7, 138.4, 136.9, 134.0, 131.4, 131.0, 128.4, 128.0, 128.0, 128.0,

124.7, 87.9, 78.8, 74.8, 65.5, 62.2, 60.0, 48.7, 39.3, 27.8, 21.6. HRMS (ESI-TOF-MS): *m/z* calcd for $C_{58}H_{52}F_{30}N_{10}O_2P_5$ $[M - PF_6]^+$ 1645.2479, observed 1645.2484; *m/z* calcd for $C_{58}H_{52}F_{24}N_{10}O_2P_4$ $[M - 2PF_6]^{2+}$ 750.1416, observed 750.1423.

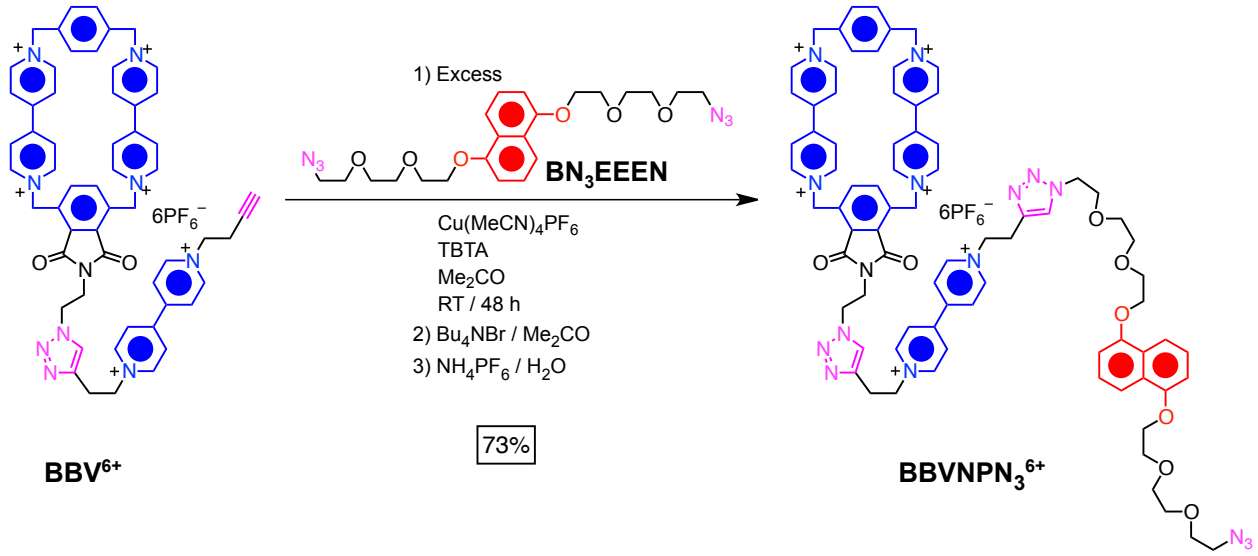


**Scheme S4**. Synthesis of daisy chain precursor **BBVNPN$_3$**·6PF$_6$

**BBVNPN$_3$·6PF$_6$**. Compounds **BN$_3$EEEN** (250 mg, 0.53 mmol) and **BBV**·6PF$_6$ (110 mg, 0.061 mmol) were dissolved in degassed $Me_2CO$ (3 mL). $Cu(MeCN)_4PF_6$ (9 mg, 0.024 mmol) and tris[(1-benzyl-1*H*-1,2,3-triazol-4-yl)methyl]amine (TBTA) (14 mg, 0.026 mmol) were added in one portion and the reaction mixture was stirred at ambient temperature for 24 h. The positively charged product was precipitated by the addition of a solution of $Bu_4NBr$ (500 mg) in $Me_2CO$ (2 mL). The precipitate was collected by centrifugation, dissolved in $H_2O$ (5 mL), and purified by preparative HPLC, eluting with $H_2O$/MeCN (0–50% MeCN in 40 min). Pure fractions were verified by analytical HPLC, combined, concentrated, and added to a saturated aqueous solution of $NH_4PF_6$ (3 mL) to afford **BBVNPN$_3$**·6PF$_6$ as a white precipitate (102 mg, 73%). $^1$H NMR (500 MHz, $CD_3CN$, 298 K) $\delta$ = 8.97 (d, $J$ = 6.6 Hz, 2H), 8.90 (d, $J$ = 6.4 Hz, 2H), 8.84 (d, $J$ = 6.2 Hz, 2H), 8.64 (d, $J$ = 6.2 Hz, 2H), 8.63 (d, $J$ = 6.6 Hz, 2H), 8.46 (s, 2H), 8.36 (d, $J$ = 6.2 Hz, 2H), 8.24 (d, $J$ = 6.2 Hz, 2H), 8.23 (d, $J$ = 6.6 Hz, 2H), 8.20 (s, 1H), 8.04 (s, 2H), 7.96 (s, 2H), 7.71 (s, 1H), 7.53 (d, $J$ = 6.7 Hz, 2H), 7.34 (d, $J$ = 6.6 Hz, 2H), 7.28 (d, $J$ = 6.4 Hz, 2H), 7.20 (d, J = 6.6 Hz, 2H), 6.34 (d, $J$ = 7.9 Hz, 1H), 6.14 (d, $J$ = 13.7 Hz, 2H), 6.11 (t, $J$ = 8.0 Hz, 1H), 6.02 (d, $J$ = 7.8 Hz, 1H), 5.75–5.72 (m, 4H), 5.71 (d, $J$ = 13.7 Hz, 2H), 5.59 (t, $J$ = 8.0 Hz, 1H), 5.07

(t, $J$ = 6.1 Hz, 2H), 4.91 (m, 2H), 4.88 (t, $J$ = 5.8 Hz, 2H), 4.42 (t, $J$ = 4.9 Hz, 2H), 4.30 (m, 2H), 4.23 (m, 2H), 4.21 (m, 2H), 4.07 (m, 2H), 4.03–3.99 (m, 4H), 3.97–3.93 (m, 4H), 3.89–3.86 (m, 4H), 3.72 (t, $J$ = 4.9 Hz, 2H), 3.62 (t, $J$ = 6.1 Hz, 2H), 3.40–3.36 (m, 4H), 2.65 (d, $J$ = 8.3 Hz, 1H), 2.36 (d, $J$ = 8.3 Hz, 1H). $^{13}$C NMR (125 MHz, $CD_3CN$, 298 K) $\delta$ = 168.2, 152.0, 151.8, 150.8, 150.3, 147.0, 146.6, 146.6, 146.4, 146.2, 145.9, 145.7, 145.1, 144.7, 143.2, 142.6, 139.6, 137.4, 134.8, 132.3, 132.1, 130.8, 129.2, 129.1, 127.9, 127.6, 127.4, 126.9, 126.5, 125.5, 125.2, 125.1, 124.6, 109.3, 107.8, 105.8, 105.5, 71.9, 71.7, 71.3, 70.6, 70.4, 70.3, 70.3, 70.2, 69.7, 69.1, 66.1, 62.5, 62.2, 59.6, 51.1, 50.4, 50.0, 40.3, 28.1, 27.2. HRMS (ESI-TOF-MS): *m/z* calcd for $C_{80}H_{82}F_{30}N_{16}O_8P_5$ $[M - PF_6]^+$ 2119.4706, observed 2120.4783; *m/z* calcd for $C_{80}H_{82}F_{24}N_{16}O_8P_4$ $[M - 2PF_6]^{2+}$ 987.2529, observed 987.2543; *m/z* calcd for $C_{80}H_{82}F_{18}N_{16}O_8P_3$ $[M - 3PF_6]^{3+}$ 610.1815, observed 610.1853.

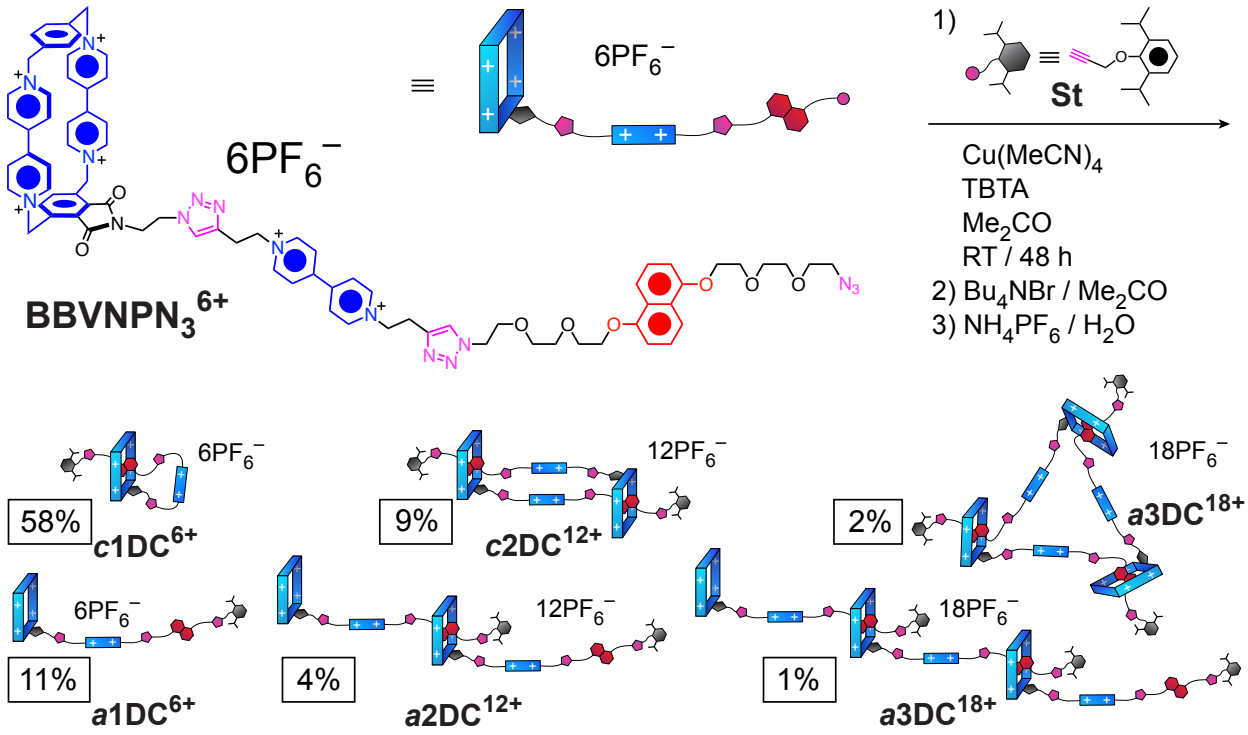


**Scheme S5**. Synthesis of blue box daisy chain compounds ***c*1DC**·6$PF_6$, ***a*1DC**·6$PF_6$, ***c*2DC**·12$PF_6$, ***a*2DC**·12$PF_6$, ***c*3DC**·18$PF_6$, and ***a*3DC**·18$PF_6$

**Synthesis of Blue Box Daisy Chains**. $Cu(MeCN)_4PF_6$ (2.5 mg, 6.7 μmol) and TBTA (3.8 mg, 7.2 μmol) were added in one portion to a degassed solution of **BBVNPN$_3$**·6$PF_6$ (39 mg, 17 μmol) and **St** (19 mg, 88 μmol) in $Me_2CO$ (1 mL). After stirring for 2 d at ambient temperature,

the positively charged products were precipitated by the addition of saturated solution of $Bu_4NBr$ in $Me_2CO$ (1 mL). The precipitate was collected by centrifugation, dissolved in $H_2O$ (2 mL), and purified by preparative HPLC, eluting in $H_2O$/MeCN (0–30% MeCN in 15 min, 30–65% MeCN in 30 min). Each fraction collected was analyzed by analytical HPLC. Pure fractions of each compound were combined, concentrated, and precipitated with a saturated aqueous solution of $NH_4PF_6$ (2 mL).

**Monomer *a*1DC·6PF$_6$** (4.6 mg, 11%). $^1$H NMR (600 MHz, $CD_3CN$, 298 K) $\delta$ = 8.85 (d, $J$ = 7.0 Hz, 4H), 8.83 (d, $J$ = 7.0 Hz, 4H), 8.80 (d, $J$ = 6.9 Hz, 2H), 8.61 (d, $J$ = 6.9 Hz, 2H), 8.24 (d, $J$ = 6.9 Hz, 2H), 8.20 (d, $J$ = 6.9 Hz, 2H), 8.19 (d, $J$ = 7.0 Hz, 4H), 8.14 (d, $J$ = 7.0 Hz, 4H), 7.98 (s, 2H), 7.93 (s, 1H), 7.69 (s, 1H), 7.66 (s, 1H), 7.65 (d, $J$ = 8.5 Hz, 1H), 7.57 (d, $J$ = 8.5 Hz, 1H), 7.46 (s, 4H), 7.28 (dd, $J$ = 7.6, 8.5 Hz, 1H), 7.22 (dd, $J$ = 7.6, 8.5 Hz, 1H), 7.15–7.10 (m, 3H), 6.84 (d, $J$ = 7.6 Hz, 1H), 6.83 (d, $J$ = 7.6 Hz, 1H), 6.11 (s, 4H), 5.74 (s, 4H), 4.93 (t, $J$ = 6.9 Hz, 2H), 4.81 (s, 2H), 4.80 (t, $J$ = 6.6 H, 2H), 4.55 (t, $J$ = 5.8 Hz, 2H), 4.52 (t, $J$ = 5.2 Hz, 2H), 4.45 (t, $J$ = 5.1 Hz, 2H), 4.22–4.19 (m, 4H), 3.92 (t, $J$ = 5.8 Hz, 2H), 3.91–3.88 (m, 6H), 3.79 (t, $J$ = 5.1 Hz, 2H), 3.71–3.69 (m, 4H), 3.66–3.64 (m, 2H), 3.62–3.60 (m, 2H), 3.45 (t, $J$ = 6.9 Hz, 2H), 3.39 (p, $J$ = 6.9 Hz, 2H), 3.29 (t, $J$ = 6.5 Hz, 2H), 1.17 (d, $J$ = 6.9 Hz, 12H). $^{13}$C NMR (125 MHz, $CDCl_3$, 298 K) $\delta$ = 168.1, 155.0, 154.9, 153.7, 150.5, 150.5, 150.4, 150.2, 146.8, 146.6, 146.4, 146.0, 144.6, 142.8, 142.7, 142.1, 138.4, 136.9, 133.9, 131.3, 131.0, 128.3, 127.9, 127.6, 127.4, 127.1, 127.0, 126.5, 126.0, 125.1, 125.0, 124.7, 124.6, 115.0, 114.8, 106.9, 106.8, 71.3, 71.2, 71.1, 70.9, 70.3, 70.3, 69.9, 69.8, 68.9, 68.9, 68.5, 65.5, 62.2, 62.1, 59.9, 50.9, 50.7, 48.6, 39.2, 27.7, 27.2, 24.2. HRMS (ESI-TOF-MS): *m/z* calcd for $C_{95}H_{102}F_{30}N_{16}O_9P_5$ $[M - PF_6]^+$ 2336.6253, observed 2336.6131; *m/z* calcd for $C_{95}H_{102}F_{24}N_{16}O_9P_4$ $[M - 2PF_6]^{2+}$ 1095.8303, observed 1095.8306; *m/z* calcd for $C_{95}H_{102}F_{18}N_{16}O_9P_3$ $[M - 3PF_6]^{3+}$ 682.2320, observed 682.2358.

**Ouroboros *c*1DC·6PF$_6$** (24.6 mg, 58%). $^1$H NMR (500 MHz, $CD_3CN$, 298 K) $\delta$ = 8.91 (d, $J$ = 6.7 Hz, 2H), 8.89 (d, $J$ = 6.7 Hz, 2H), 8.87 (d, $J$ = 6.2 Hz, 2H), 8.64 (d, $J$ = 6.2 Hz, 2H), 8.60 (d, $J$ = 6.5 Hz, 2H), 8.45 (s, 2H), 8.36 (d, $J$ = 6.2 Hz, 2H), 8.24 (d, $J$ = 6.2 Hz, 2H), 8.23 (d, $J$ = 6.5 Hz, 2H), 8.19 (s, 1H), 7.95 (s, 2H), 7.92 (s, 2H), 7.90 (s, 1H), 7.70 (s, 1H), 7.54 (dd, $J$ = 2.4, 6.5 Hz, 2H), 7.32 (dd, $J$ = 2.4, 6.5 Hz, 2H), 7.27 (dd, $J$ = 2.4, 6.7 Hz, 2H), 7.17 (dd, $J$ = 2.4, 6.7 Hz, 2H), 7.16–7.10 (m, 3H), 6.33 (d, $J$ = 8.0 Hz, 1H), 6.14 (d, $J$ = 13.6 Hz, 2H), 6.09 (t, $J$ = 8.0 Hz, 1H), 6.01 (d, $J$ = 8.0 Hz, 1H), 5.73 (d, $J$ = 13.6 Hz, 2H), 5.64 (d, $J$ = 13.6 Hz, 2H), 5.60 (d, $J$ =

13.6 Hz, 2H), 5.57 (d, $J$ = 8.0, 1H), 5.07 (t, $J$ = 6.1 Hz, 2H), 4.91 (t, $J$ = 6.1 Hz, 2H), 4.88 (t, $J$ = 5.8 Hz, 2H), 4.66 (s, 2H), 4.52 (t, $J$ = 5.1 Hz, 2H), 4.41 (t, $J$ = 4.8 Hz, 2H), 4.30 (m, 2H), 4.23 (m, 2H), 4.20 (m, 2H), 4.04–3.86 (m, 16H), 3.61 (t, $J$ = 6.1 Hz, 2H), 3.37 (t, $J$ = 5.8 Hz, 2H), 3.31 (hep, $J$ = 7.0 Hz, 2H), 2.66 (d, $J$ = 8.0 Hz, 1H), 2.31 (d, $J$ = 8.0 Hz, 1H), 1.15 (d, $J$ = 7.0 Hz, 12H). $^{13}$C NMR (125 MHz, $CD_3CN$, 298K) $\delta$ = 168.3, 153.6, 155.3, 150.9, 146.7, 146.7, 146.4, 146.4, 146.2, 145.8, 145.7, 145.0, 145.0, 144.7, 144.7, 143.1, 142.8, 142.6, 139.6, 139.6, 137.4, 134.8, 132.3, 132.0, 130.8, 129.2, 129.1, 127.9, 127.6, 127.4, 126.9, 126.5, 126.0, 125.4, 125.1, 125.2, 125.0, 124.8, 124.6, 109.3, 107.8, 105.9, 105.5, 71.8, 71.7, 71.2, 70.6, 70.4, 70.2, 70.2, 70.1, 69.7, 69.4, 69.0, 68.3, 62.6, 62.2, 59.6, 54.1, 50.5, 50.4, 50.0, 40.3, 30.8, 27.2, 24.2. HRMS (ESI-TOF-MS): *m/z* calcd for $C_{95}H_{102}F_{30}N_{16}O_9P_5$ $[M - PF_6]^+$ 2336.6253, observed 2336.6552; *m/z* calcd for $C_{95}H_{102}F_{24}N_{16}O_9P_4$ $[M - 2PF_6]^{2+}$ 1095.8303, observed 1095.8322; *m/z* calcd for $C_{95}H_{102}F_{18}N_{16}O_9P_3$ $[M - 3PF_6]^{3+}$ 682.2320, observed 682.2357.

**[*c*2]Daisy Chain *c*2DC·12PF$_6$** (3.7 mg, 9%). $^1$H NMR (500 MHz, $CD_3CN$, 298 K) $\delta$ = 8.99 (d, $J$ = 6.7 Hz, 4H), 8.93 (d, $J$ = 6.7 Hz, 4H), 8.88 (d, $J$ = 6.5 Hz, 4H), 8.77 (d, $J$ = 6.5 Hz, 4H), 8.63 (d, $J$ = 6.7 Hz, 4H), 8.52 (d, $J$ = 6.7 Hz, 4H), 8.40 (d, $J$ = 6.5 Hz, 4H), 8.36 (d, $J$ = 6.5 Hz, 4H), 8.35 (s, 4H), 7.97 (s, 4H), 7.93 (s, 4H), 7.90 (s, 2H), 7.73 (s, 2H), 7.64 (s, 2H), 7.59 (d, $J$ = 6.7 Hz, 4H), 7.38 (d, $J$ = 6.7 Hz, 4H), 7.26 (d, $J$ = 6.7 Hz, 4H), 7.20 (d, $J$ = 6.7 Hz, 4H), 7.15–7.09 (m, 6H), 6.46 (d, $J$ = 14.0 Hz, 4H), 6.32 (d, $J$ = 8.1 Hz, 2H), 6.26 (d, $J$ = 8.0 Hz, 2H), 6.07 (t, $J$ = 8.2 Hz, 2H), 5.67 (d, $J$ = 13.8 Hz, 4H), 5.62 (d, $J$ = 13.8 Hz, 4H), 5.61 (d, $J$ = 8.0, 2H), 5.61 (d, $J$ = 14.0 Hz, 4H), 4.97 (t, $J$ = 6.6 Hz, 4H), 4.85–4.80 (m, 8H), 4.65 (s, 4H), 4.52 (m, 4H), 4.47 (m, 4H), 4.24–3.87 (m, 44H), 3.52 (t, $J$ = 6.6 Hz, 4H), 3.30 (hep, $J$ = 6.9 Hz, 4H), 3.09 (m, 4H), 2.60 (d, $J$ = 8.1 Hz, 2H), 2.35 (d, $J$ = 8.2 Hz, 2H), 1.15 (d, $J$ = 6.9 Hz, 24H). $^{13}$C NMR (125 MHz, $CD_3CN$, 298K) $\delta$ = 168.2, 153.7, 151.9, 151.1, 146.8, 146.7, 146.7, 146.5, 145.8, 145.8, 145.1, 145.0, 144.9, 144.8, 143.4, 142.8, 142.4, 139.5, 137.4, 135.0, 134.9, 132.3, 132.1, 130.8, 129.3, 128.9, 128.0, 128.0, 127.9, 127.4, 127.1, 126.3, 126.1, 125.6, 125.3, 125.1, 125.1, 124.9, 118.3, 109.4, 107.9, 106.1, 105.6, 72.1, 71.9, 71.3, 70.8, 70.4, 70.2, 70.1, 69.3, 69.2, 68.3, 66.1, 66.1, 62.5, 62.0, 59.7, 59.5, 50.5, 50.2, 49.9, 46.0, 40.5, 27.3, 24.3. HRMS (ESI-TOF-MS): *m/z* calcd for $C_{190}H_{204}F_{60}N_{32}O_{18}P_{10}$ $[M - 2PF_6]^{2+}$ 2336.6253, observed 2336.6274; *m/z* calcd for $C_{190}H_{204}F_{54}N_{32}O_{18}P_9$ $[M - 3PF_6]^{3+}$ 1509.4286, observed 1509.4334; *m/z* calcd for $C_{190}H_{204}F_{48}N_{32}O_{18}P_8$ $[M - 4PF_6]^{4+}$ 1095.8303, observed 1095.8298.

**[*a*2]Daisy Chain *a*2DC·12PF$_6$** (1.7 mg, 4%). $^1$H NMR (600 MHz, $CD_3CN$, 353 K) $\delta$ = 8.93 (d, $J$ = 6.7 Hz, 2H), 8.90 (d, $J$ = 7.0 Hz, 2H), 8.88 (d, $J$ = 6.7 Hz, 2H), 8.88 (d, $J$ = 6.7 Hz, 4H), 8.83 (br s, 8H), 8.81 (d, $J$ = 6.7 Hz, 4H), 8.70 (d, $J$ = 6.8 Hz, 2H), 8.47 (s, 2H), 8.39 (d, $J$ = 7.0 Hz, 2H), 8.37 (d, $J$ = 6.7 Hz, 2H), 8.36 (d, $J$ = 6.5 Hz, 2H), 8.30 (d, $J$ = 6.7 Hz, 2H), 8.19 (d, $J$ = 6.7 Hz, 4H), 8.18 (d, $J$ = 6.7 Hz, 4H), 8.03 (s, 4H), 8.01 (s, 2H), 7.87 (s, 1H), 7.86 (s, 1H), 7.86 (s, 1H), 7.78 (d, $J$ = 8.5 Hz, 1H), 7.74 (d, $J$ = 8.5 Hz, 1H), 7.72 (s, 1H), 7.68 (s, 1H), 7.67 (s, 1H), 7.47 (br s, 4H), 7.44 (s, 4H), 7.36 (br s, 4H), 7.35 (t, $J$ = 8.5 Hz, 1H), 7.32 (t, $J$ = 8.5 Hz, 1H), 7.16–7.10 (m, 6H), 6.94 (d, $J$ = 8.5 Hz, 1H), 6.94 (d, $J$ = 8.5 Hz, 1H), 6.42 (d, $J$ = 8.0 Hz, 1H), 6.42 (d, $J$ = 8.0 Hz, 1H), 6.24 (br s, 4H), 6.20 (s, 4H), 5.92 (br s, 2H), 5.78 (s, 4H), 5.75 (s, 4H), 5.02 (t, $J$ = 7.0 Hz, 2H), 5.01 (t, $J$ = 7.0 Hz, 2H), 4.95 (t, $J$ = 7.0 Hz, 2H), 4.91 (t, $J$ = 7.0 Hz, 2H), 4.89 (s, 2H), 4.89 (t, $J$ = 7.0 Hz, 2H), 4.82 (s, 2H), 4.63 (t, $J$ = 6.2 Hz, 2H), 4.55 (t, $J$ = 5.3 Hz, 2H), 4.52 (t, $J$ = 5.3 Hz, 2H), 4.50 (t, $J$ = 5.3 Hz, 2H), 4.45 (t, $J$ = 5.3 Hz, 2H), 4.36–4.33 (m, 4H), 4.31 (m, 2H), 4.29–4.27 (m, 4H), 4.19–4.16 (m, 4H), 4.08 (t, $J$ = 5.3 Hz, 2H), 4.04–4.00 (m, 8H), 3.95–3.90 (m, 10H), 3.85 (t, $J$ = 5.3 Hz, 2H), 3.72–3.70 (m, 4H), 3.66 (dd, $J$ = 3.5, 5.8 Hz, 2H), 3.63 (dd, $J$ = 3.5, 5.8 Hz, 2H), 3.57 (t, $J$ = 7.0 Hz, 2H), 3.51 (t, $J$ = 7.0 Hz, 2H), 3.42 (hep, $J$ = 6.9 Hz, 2H), 3.39–3.35 (m, 4H), 3.37 (hep, $J$ = 6.9 Hz, 2H), 2.66 (d, $J$ = 8.2 Hz, 2H), 1.21 (d, $J$ = 6.9 Hz, 12H), 1.20 (d, $J$ = 6.9 Hz, 12H). HRMS (ESI-TOF-MS): *m/z* calcd for $C_{190}H_{204}F_{60}N_{32}O_{18}P_{10}$ $[M - 2PF_6]^{2+}$ 2336.6253, observed 2336.6435; *m/z* calcd for $C_{190}H_{204}F_{54}N_{32}O_{18}P_9$ $[M - 3PF_6]^{3+}$ 1509.4286, observed 1509.4279; *m/z* calcd for $C_{190}H_{204}F_{48}N_{32}O_{18}P_8$ $[M - 4PF_6]^{4+}$ 1095.8303, observed 1095.8301; *m/z* calcd for $C_{190}H_{204}F_{42}N_{32}O_{18}P_7$ $[M - 5PF_6]^{5+}$ 847.6713, observed 847.6773.

**[*c*3]Daisy Chain *c*3DC·18PF$_6$** (0.7 mg, 2%). $^1$H NMR (600 MHz, $CD_3CN$, 353 K) $\delta$ = 8.93 (d, $J$ = 6.5 Hz, 6H), 8.85 (d, $J$ = 6.5 Hz, 6H), 8.84 (br s, 24H), 8.48 (s, 6H), 8.42 (d, $J$ = 6.5 Hz, 6H), 8.37 (d, $J$ = 6.5 Hz, 6H), 8.03 (s, 12H), 7.88 (s, 3H), 7.84 (s, 3H), 7.65 (s, 3H), 7.49 (br s, 12H), 7.36 (br s, 12H), 7.16–7.10 (m, 9H), 6.43 (d, $J$ = 8.0 Hz, 3H), 6.42 (d, $J$ = 8.0 Hz, 3H), 6.23 (br s, 12H), 5.92 (br s, 6H), 5.76 (s, 12H), 5.04 (t, $J$ = 6.9 Hz, 6H), 4.93 (t, $J$ = 6.9 Hz, 6H), 4.88 (m, 6H), 4.82 (s, 6H), 4.56 (t, $J$ = 5.3 Hz, 6H), 5.33 (t, $J$ = 5.3 Hz, 6H), 4.36–4.32 (m, 12H), 4.27 (m, 6H), 4.19–4.16 (m, 12H), 4.08 (t, $J$ = 5.3 Hz, 6H), 4.03–3.99 (m, 18H), 3.94 (m, 6H), 3.91 (t, $J$ = 4.3 Hz, 6H), 3.58 (t, $J$ = 6.9 Hz, 6H), 3.37 (hep, $J$ = 6.9 Hz, 6H), 3.33 (t, $J$ = 6.9 Hz, 6H), 2.66 (br s, 6H), 1.20 (d, $J$ = 6.9 Hz, 36H). HRMS (ESI-TOF-MS): *m/z* calcd for

$C_{285}H_{306}F_{90}N_{48}O_{27}P_{15}$ $[M - 3PF_6]^{3+}$ 2336.6253, observed 2336.6349; *m/z* calcd for $C_{285}H_{306}F_{84}N_{48}O_{27}P_{14}$ $[M - 4PF_6]^{4+}$ 1716.2278, observed 1716.2111; *m/z* calcd for $C_{285}H_{306}F_{78}N_{48}O_{27}P_{13}$ $[M - 5PF_6]^{5+}$ 1343.9890, observed 1343.9868.

**[*a*3]Daisy Chain *a*3DC·18PF$_6$** (0.3 mg, 1%). HRMS (ESI-TOF-MS): *m/z* calcd for $C_{285}H_{306}F_{90}N_{48}O_{27}P_{15}$ $[M - 3PF_6]^{3+}$ 2336.6253, observed 2336.6262; *m/z* calcd for $C_{285}H_{306}F_{84}N_{48}O_{27}P_{14}$ $[M - 4PF_6]^{4+}$ 1716.2278, observed 1716.2740; *m/z* calcd for $C_{285}H_{306}F_{78}N_{48}O_{27}P_{13}$ $[M - 5PF_6]^{5+}$ 1343.9890, observed 1343.9834.

### 3. Mass Spectrometry of Blue Box Daisy Chains

Selected signals observed for the daisy chains by ESI-MS are compared with their calculated isotope patterns in Figure S1. All of the signals are in good agreement with predictions.

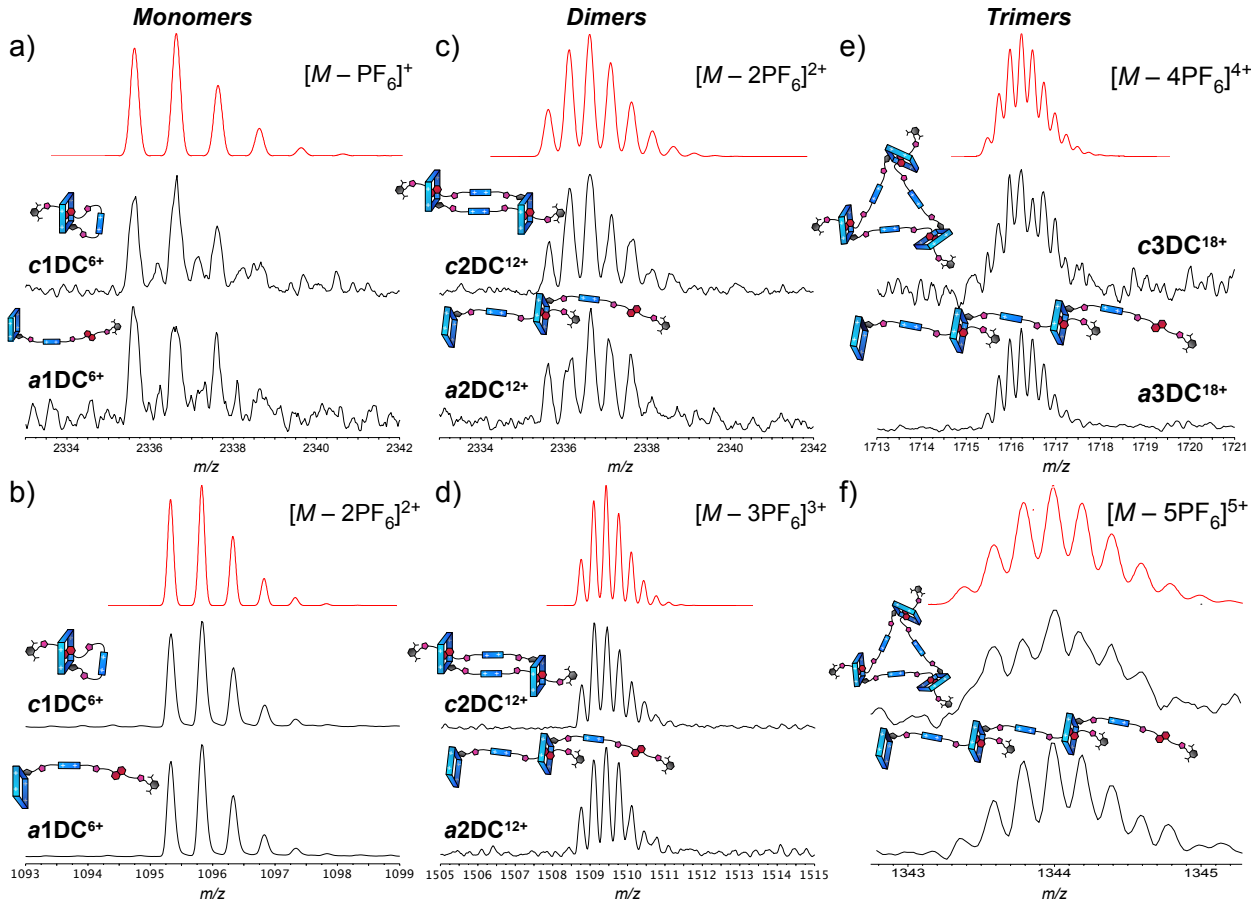


**Figure S1**. The observed ESI-MS signals (black) compared with the corresponding calculated signals (red) for the $[M - nPF_6]^{n+}$ ions of the blue box daisy chain monomers (a,b), dimers (c,d), and trimers (e,f)

## 4. Analysis of the $^1$H NMR Spectra of Blue Box Daisy Chains

The daisy chains were characterized using variable temperature (VT) $^1$H NMR spectroscopy as well as two-dimensional proton correlation techniques, namely $^1$H–$^1$H gradient-selected correlation spectroscopy (gCOSY) and $^1$H–$^1$H gradient-selected nuclear Overhauser effect spectroscopy (gNOESY).

### 4.1. $^1$H NMR Spectroscopic Analysis of Monomer *a*1DC·6PF$_6$

Compound ***a*1DC**$^{6+}$ has the simplest $^1$H NMR spectrum (Figure S2) on account of its high symmetry and lack of a recognition unit inside the cyclophane. In contrast with the analogues in which the ring is occupied by a DNP unit, a single set of resonances is observed and all the resonances are sharp and well-resolved across the measurable range of temperatures in $CD_3CN$.

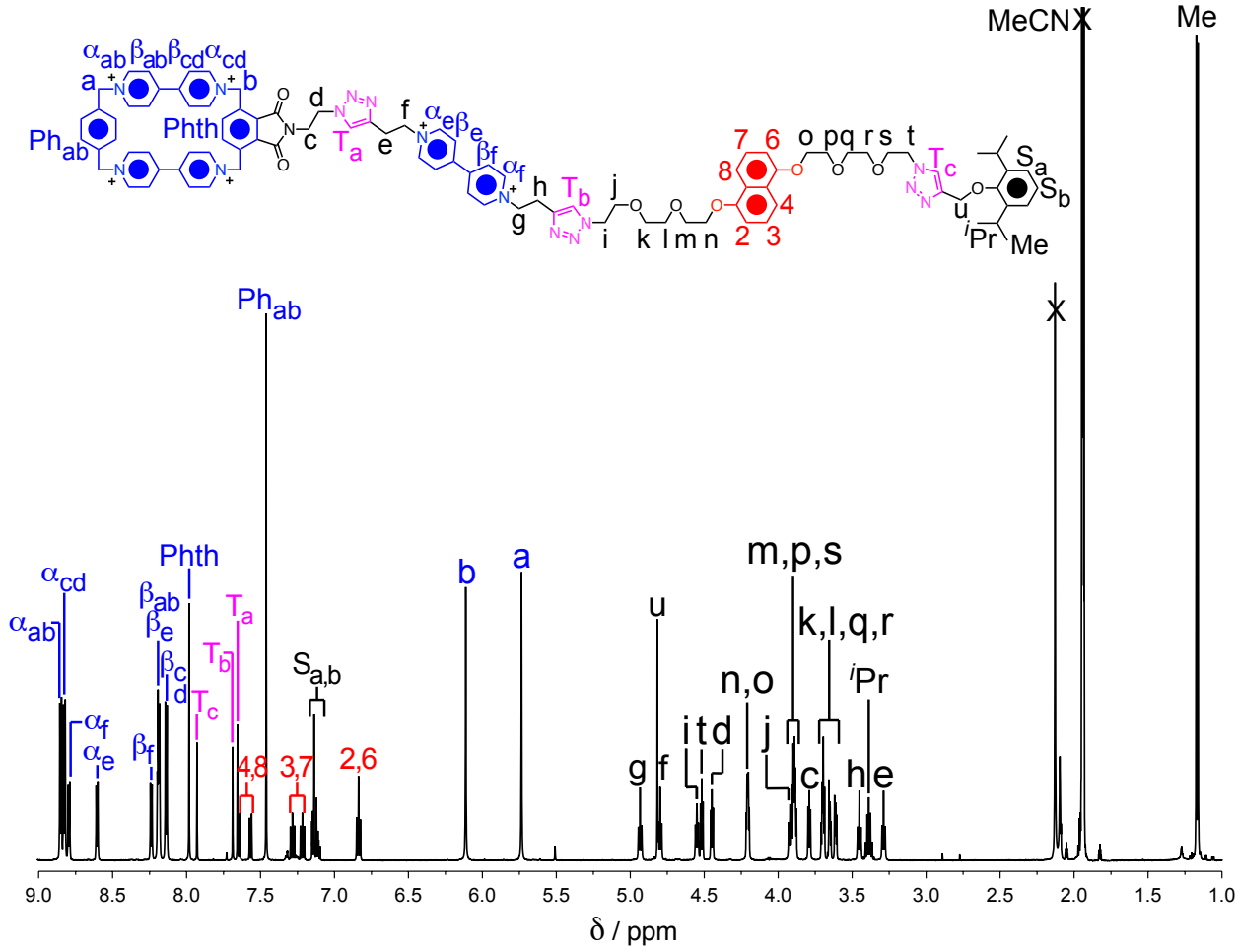


**Figure S2**. $^1$H NMR Spectrum (600 MHz, $CD_3CN$, 298 K) of monomer ***a*1DC**·6PF$_6$

The $^1$H NMR spectrum of ***a*1DC$^{6+}$** can be interpreted on the assumption that the molecule has time-averaged $C_{2v}$ symmetry as a result of the rapid free rotation of the aromatic units on the $^1$H NMR timescale. The signals were fully assigned to their corresponding protons by identifying important through-bond and through-space correlations in the $^1$H–$^1$H gCOSY (Figure S3) and gNOESY (Figure S4) spectra, respectively. Protons H$\alpha_e$ on the viologen unit are of interest because they resonate at substantially lower frequency than the other α protons, most likely as a consequence of weak side-on interactions with the free DNP unit and its appended flexible polyether chains.

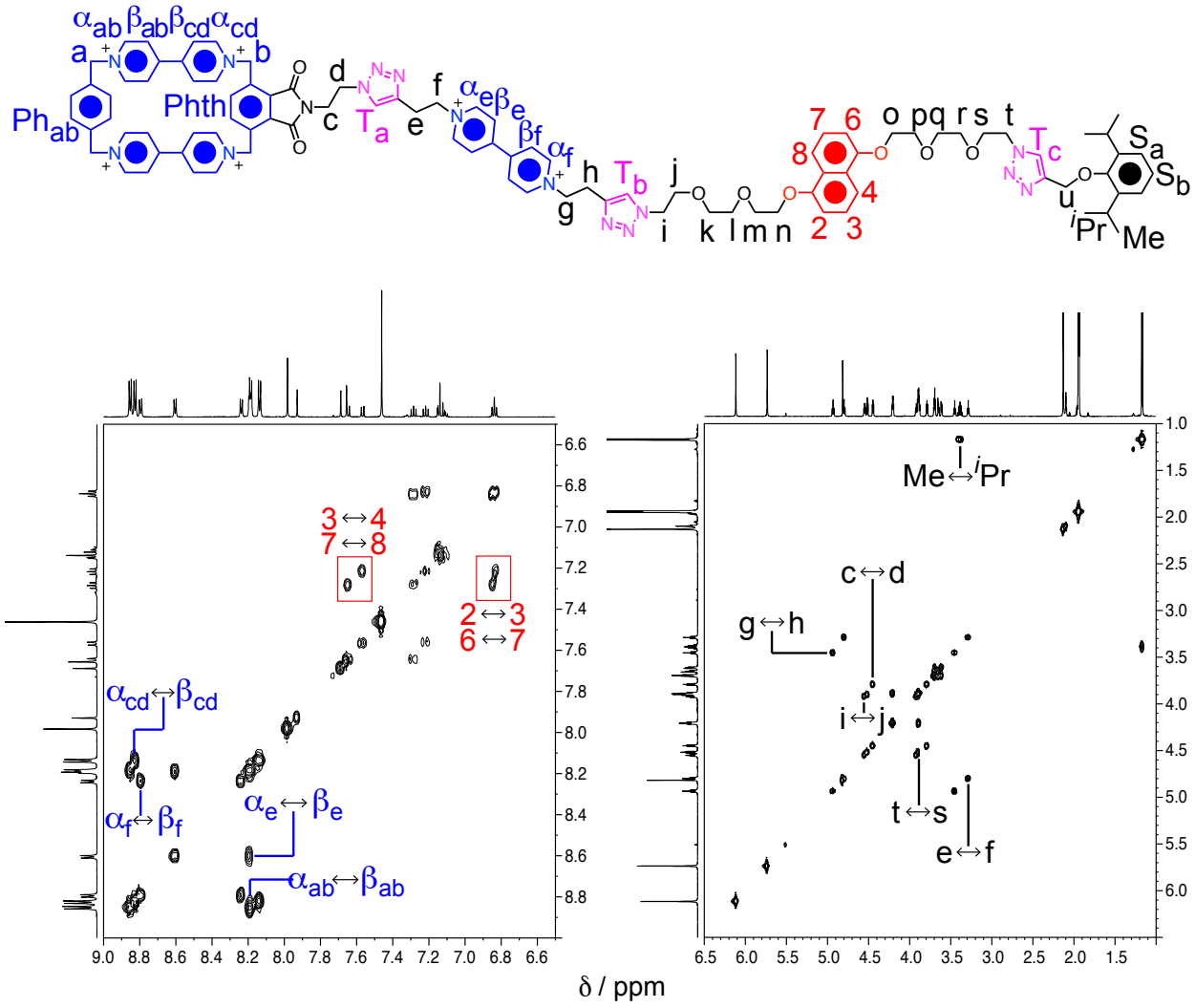


**Figure S3**. $^1$H–$^1$H gCOSY Spectrum (600 MHz, $CD_3CN$, 298 K) of monomer ***a*1DC**·6$PF_6$

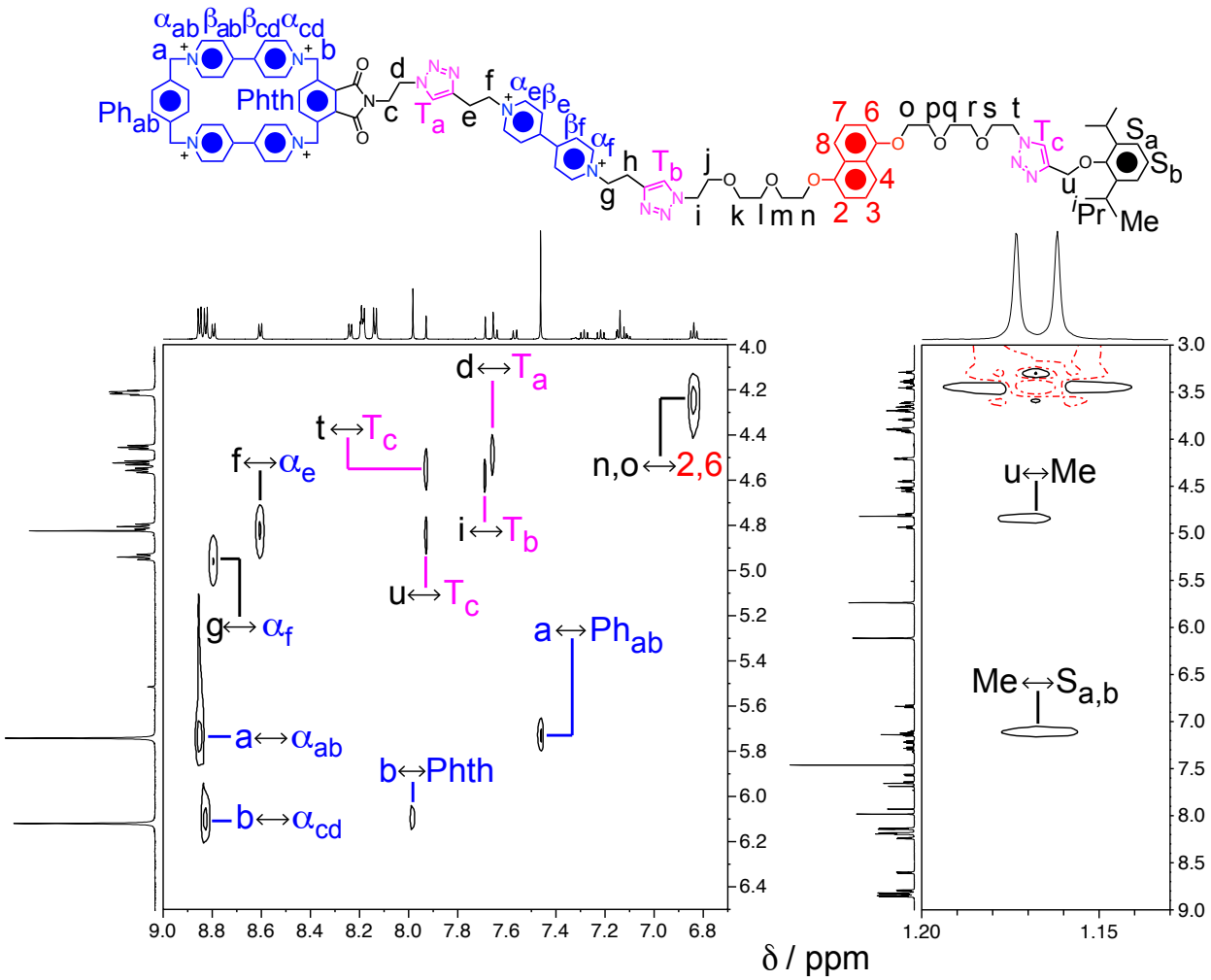


**Figure S4**. Partial $^{1}$H–$^{1}$H gNOESY spectrum (600 MHz, $CD_3CN$, 298 K) of ***a*1DC**·6$PF_6$

### 4.2. $^{1}$H NMR Spectroscopic Analysis of Ouroboros *c*1DC·6$PF_6$

The presence of a DNP guest inside the cyclophane's cavity in compound ***c*1DC**$^{6+}$ complicates its $^{1}$H NMR spectrum compared to that of ***a*1DC**$^{6+}$ because the asymmetry of the guest is imposed on the cyclophane, while preventing the rotation of its phenylene and bipyridinium units on the $^{1}$H NMR timescale. The $^{1}$H NMR spectrum of ***c*1DC**$^{6+}$ can be interpreted with the time-averaged solution-state structure of the molecule having $C_s$ symmetry, i.e., with a plane of symmetry running through the cyclophane's cavity that is coplanar with the DNP unit. Having a guest with local constitutional asymmetry inside the cavity of the cyclophane differentiates the protons around each rim of the cyclophane, which doubles the number of α, β, methylene and phenylene BB$^{4+}$ signals with respect to the free species. It is well-established[S7] that DNP units occupy the cavity of BB$^{4+}$ rings with their 4/8 protons pointing directly into the faces of the

*para*-phenylene rings as a result of [C–H···π] interactions, causing the dramatic (>5 ppm) shifts of the corresponding signals to much lower frequencies, i.e., higher fields. Thus, compound ***c*1DC**$^{6+}$ can access (Process I) two co-conformations associated with the two different orientations of the DNP unit – one in which H-4 points towards the phthalimide (Phth) unit ('*DNP-Down*'), and another one with H-4 directed into the phenylene (Ph) ring instead ('*DNP-Up*'). The two possible co-conformations of the Phth unit also differentiate ***c*1DC**$^{6+}$ into '*Phth-In*' and '*Phth-Out*' isomers by Process II. The $^{1}$H NMR spectrum (Figure S5) of ***c*1DC**$^{6+}$ shows two sets of signals with one set being much more dominant than the other, revealing that (i) one of these two processes is forbidden and (ii) one co-conformation is significantly more favored than the other one in $CD_3CN$ at 25 °C. A two-dimensional analysis (Figures S6 and S7) suggests that the dominant co-conformation is the species in which H-8 is directed into the Phth unit, *DNP-Up*. Based on the integration of the H-4/8 DNP $^{1}$H NMR signals, the two co-conformations are present (Scheme S6) in a 1:6 ratio. at 25 °C .

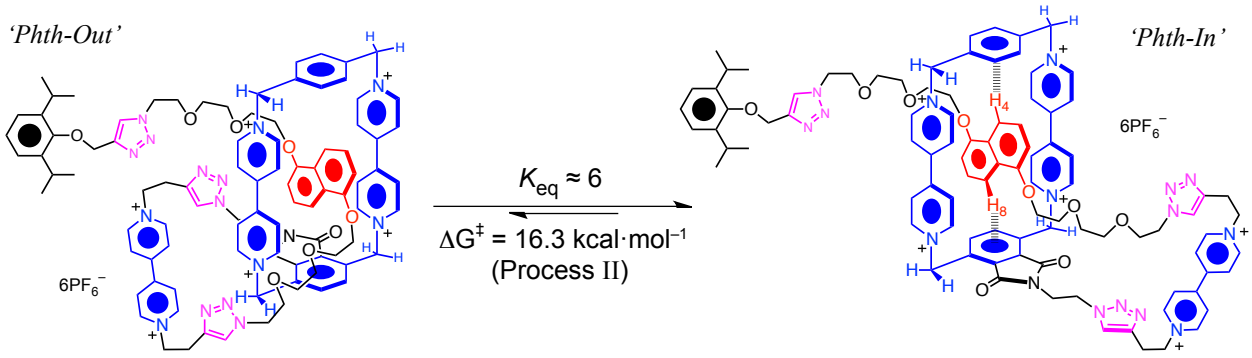


**Scheme S6**. Equilibration of the two co-conformations (*Phth-Out* and *Phth-In*) of ***c*1DC**·6PF$_6$ associated with rotation of the Phth unit (Process II).

The assignments in Figure S5 were made by identifying the signals corresponding to the phenylene/phthalimide protons (Ph$_{a,b}$ and Phth) and the triazole protons (T$_a$–T$_c$), which are easily distinguished by their singlet resonances and integrals, then following their corresponding through-space correlations between the H-4/H-8 DNP protons and BB$^{4+}$ methylene protons (H$_a$ and H$_b$) in the case of Ph and Phth protons, or methylene protons H$_d$, H$_e$, H$_h$, H$_i$, H$_t$, and H$_u$ in the case of T$_a$–T$_c$ (Figure S7). The through-bond coupling identified by the gCOSY spectrum (Figure S6) was used to make most of the remaining assignments.

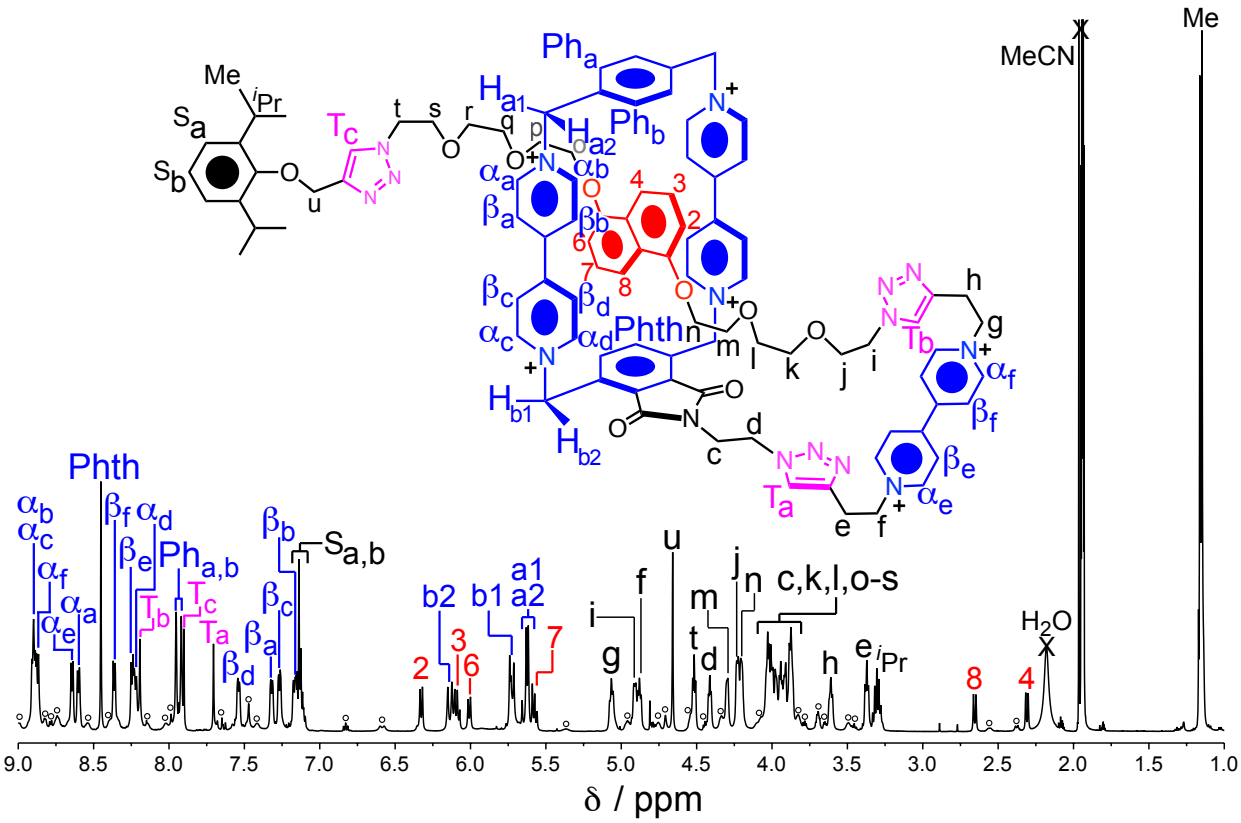


**Figure S5**. $^1$H NMR Spectrum (500 MHz, $CD_3CN$, 298 K) of ***c*1DC**·6$PF_6$. Signals corresponding to the minor '*Phth-Out*' co-conformation are labeled with open circles.

We were able to assign the major set of signals to a specific co-conformation by following a series of nuclear Overhauser effect (nOe) correlations from DNP to Phth, then from Phth to the nearest blue box methylene proton ($H_b$), and finally from $H_b$ to the adjacent α proton. Each co-conformation has a unique combination of these three correlations (Table S1). Based on the NOESY data, the most self-consistent assignment for the observed correlations is H-8↔Phth, Phth↔H-b1, H-b1↔H-$\alpha_c$ (annotated in the structure in Figure S7), corresponding to the *DNP-Up/Phth-In* co-conformation. This assignment is the most self-consistent option since we have shown[S8] that the α protons nearest in space to the polyether chain of the DNP unit resonate at significantly lower frequencies than the opposing α protons which are not in close proximity to the polyether chains, since they are stabilized by [C–H···O] hydrogen bonding interactions. Since the relevant $H_b$↔Hα correlation is the highest frequency α resonance, we can rule out the *DNP-Down/Phth-In* and *DNP-Up/Phth-Out* co-conformations, which have a polyether chain in close proximity to the α proton nearest in space to the Phth proton. Of the remaining two

options, *DNP-Up/Phth-In* is more likely because *DNP-Down/Phth-Out* will be destabilized by electrostatic repulsion from its $BIPY^{2+}$ recognition unit in much closer proximity to $BB^{4+}$.

**Table S1**. The Signatures of Expected NOE Correlations that are Unique to Each Possible Co-conformation of ***a*1DC**$^{6+}$.

| | 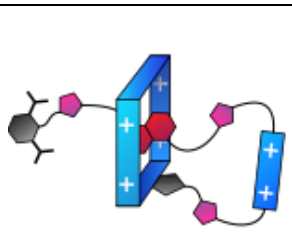 *DNP-Up/Phth-In* | 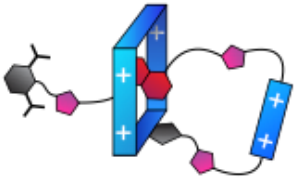 *DNP-Down/Phth-In* |  *DNP-Up/Phth-Out* |  *DNP-Down/Phth-Out* |
|---|---|---|---|---|
| $H_{DNP}$↔Phth | H-8↔Phth | H-4↔Phth | H-8↔Phth | H-4↔Phth |
| Phth↔$H_b$ | Phth↔H-b1 | Phth↔H-b1 | Phth↔H-b2 | Phth↔H-b2 |
| $H_b$↔Hα | $H_{b1}$↔H-$\alpha_c$ | $H_{b1}$↔H-$\alpha_c$ | $H_{b2}$↔H-$\alpha_d$ | $H_{b2}$↔H-$\alpha_d$ |

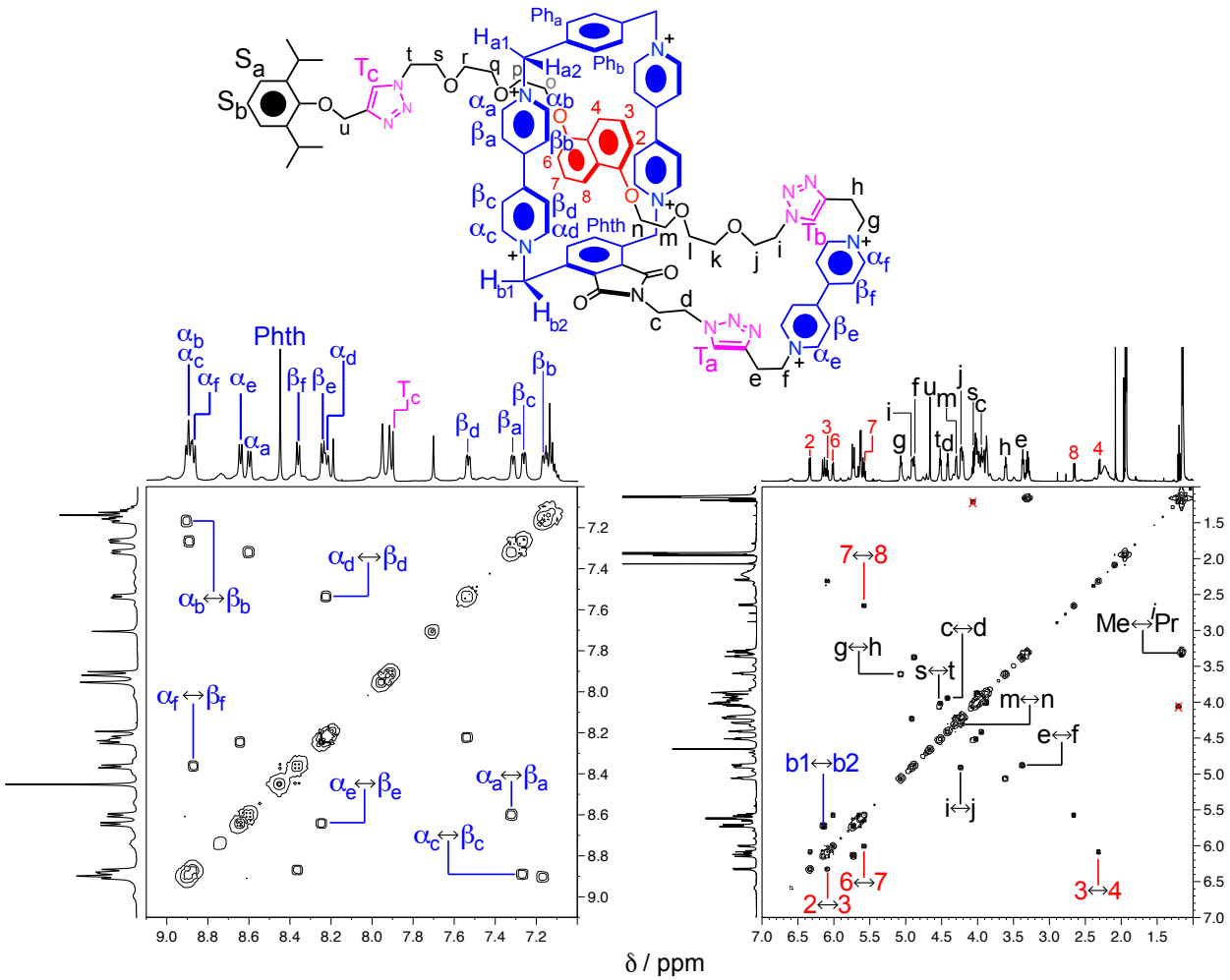


**Figure S6**. $^1H$–$^1H$ gCOSY Spectrum (500 MHz, $CD_3CN$, 298 K) of ouroboros ***c*1DC**·$6PF_6$

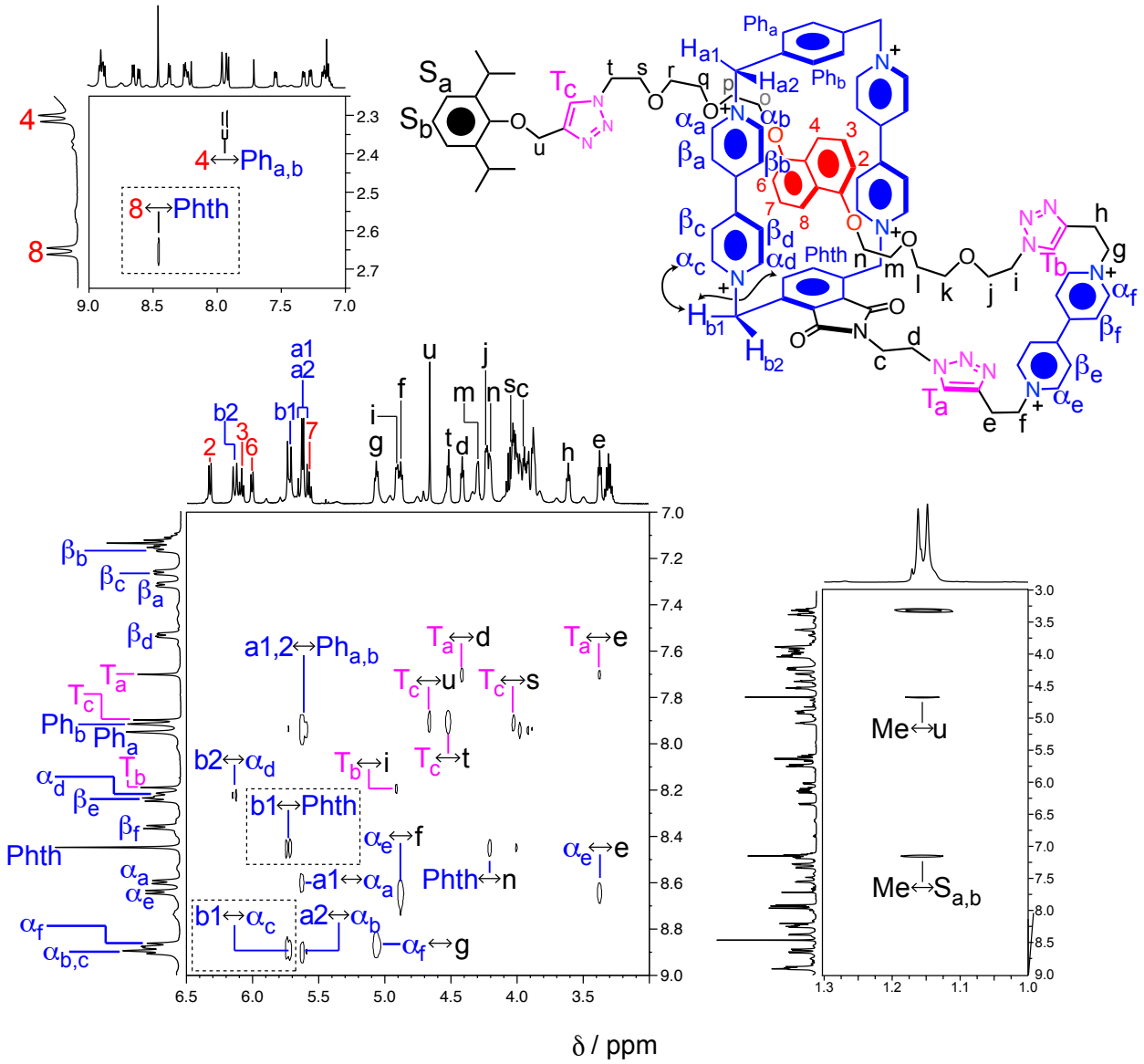


**Figure S7**. Partial $^{1}$H–$^{1}$H gNOESY Spectrum (500 MHz, $CD_3CN$, 298 K) of ouroboros ***c*1DC**·6$PF_6$

In the VT $^{1}$H NMR spectrum of ***c*1DC**$^{6+}$ in $CD_3CN$ (Figure S8), the four sharp and well-resolved H-4/8 DNP signals observed at low temperatures begin to coalesce and broaden at high temperatures until the broadest signals are detected at $T_c$ = 60 °C, above which only two signals remain, which become sharp and approach each other with increasing temperature. The other signals associated with DNP⊂BB$^{4+}$ are differentiated at low temperature and coalesce at high temperatures.

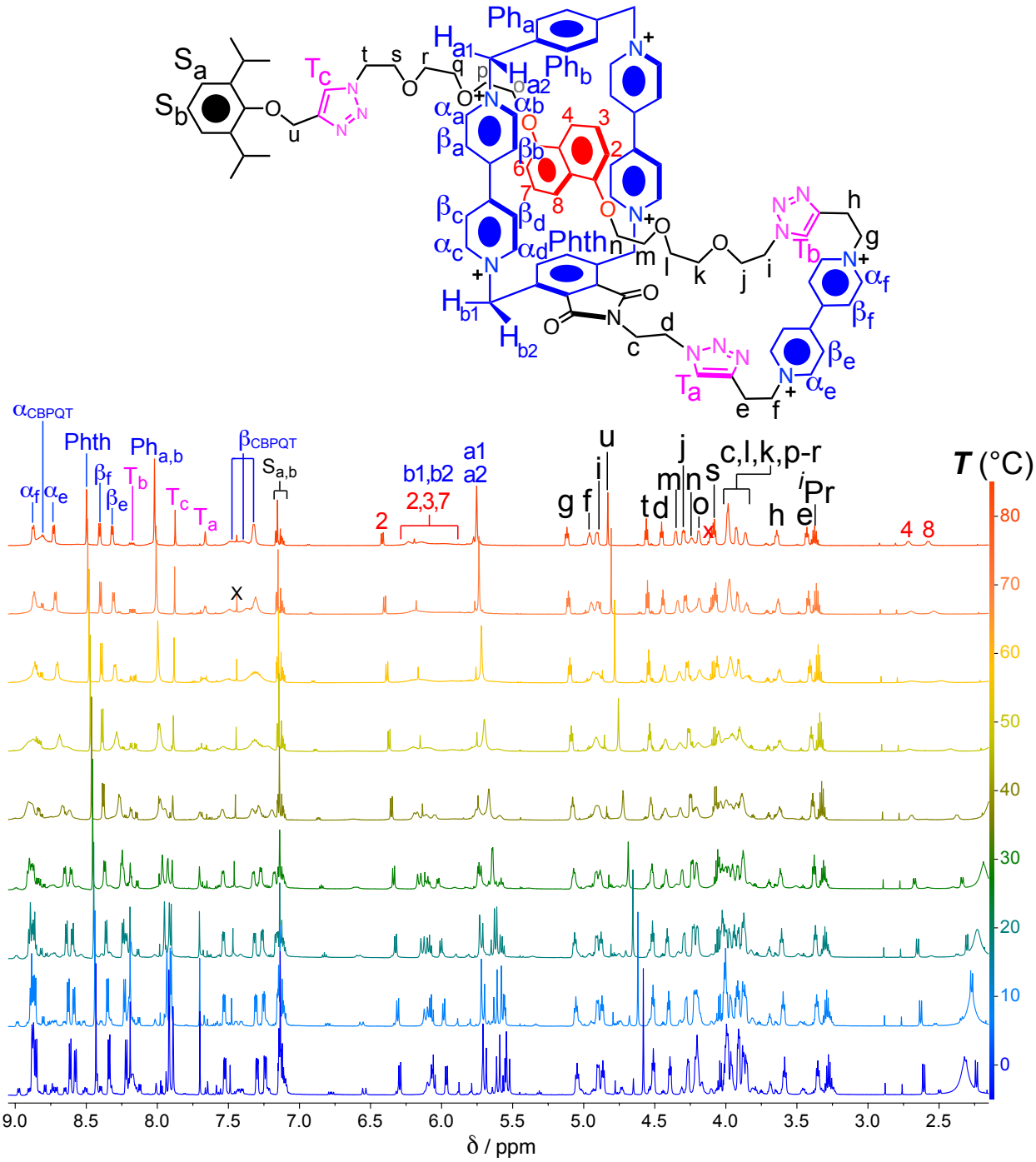


**Figure S8**. VT $^{1}$H NMR Spectrum (600 MHz, $CD_3CN$) of ***c*1DC**·6$PF_6$

### 4.3. $^{1}$H NMR Spectroscopic Analysis of [*c*2]Daisy Chain *c*2DC·12$PF_6$

Although the [*c*2]daisy chain ***c*2DC**$^{12+}$ formally has higher time-averaged symmetry than the ouroboros ***c*1DC**$^{6+}$ on account of its $C_2$ axis perpendicular to the long axis of the molecule, the $^{1}$H NMR spectrum of ***c*2DC**$^{12+}$ reveals more signals than ***c*1DC**$^{6+}$ simply because it exists as a

number of co-conformational isomers that are exchanging slowly on the $^1$H NMR timescale. Whereas only four signals were observed for the H-4/8 DNP protons of ***c*1DC$^{6+}$**, many more H-4/8 DNP signals can be observed at low temperatures in the case of ***c*2DC$^{12+}$** – as demonstrated in the partial VT $^1$H NMR spectrum in Figure S9 – revealing that both DNP rotation (process I) and Phth rotation (process II) are allowed in this daisy chain.

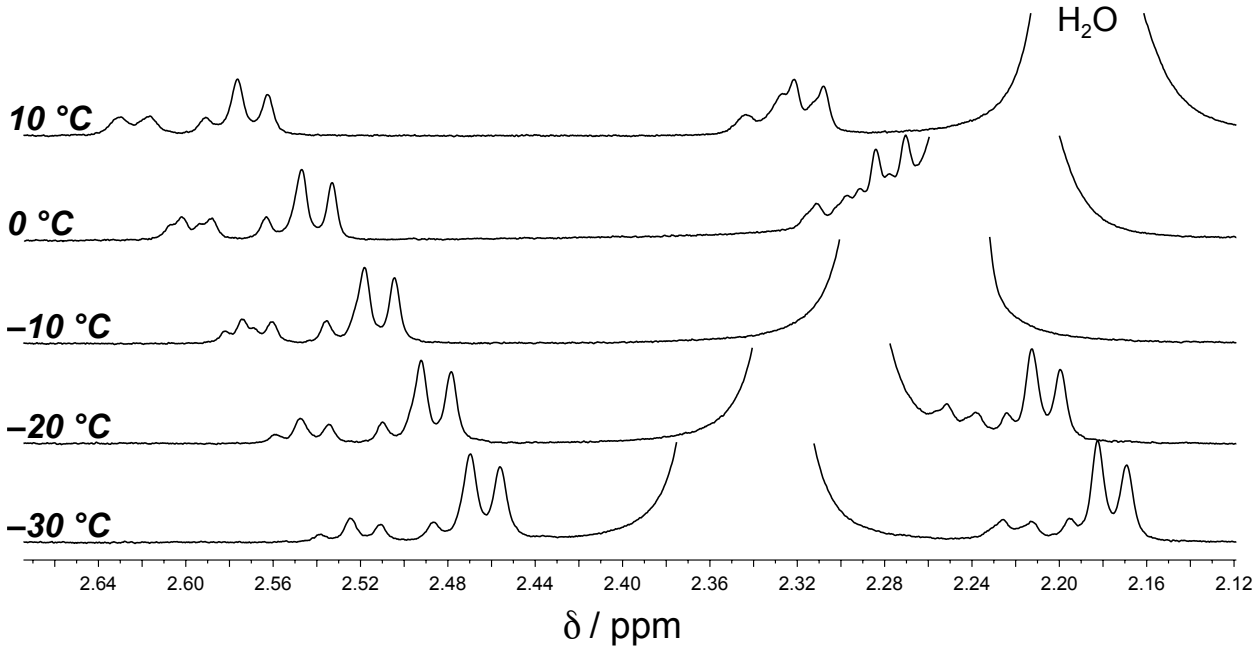


**Figure S9**. The partial VT $^1$H NMR spectrum (600 MHz, $CD_3CN$) of ***c*2DC$^{12+}$** over the temperature range of 10 to –30 °C reveals multiple overlapping 4/8 DNP signals.

The isomerism exhibited by ***c*2DC$^{12+}$** is significantly more complicated than that of ***c*1DC$^{6+}$**. Since there are two DNP⊂BB$^{4+}$ complexes that can each access $2^2 = 4$ co-conformations on account of binary Processes I and II, a total of $4^2 = 16$ co-conformations are possible. Six pairs of isomers are rendered equivalent, however, by a $C_2$ axis of symmetry. Strictly speaking, up to 10 unique co-conformational isomers (Scheme S7) are present in the equilibrium mixture.

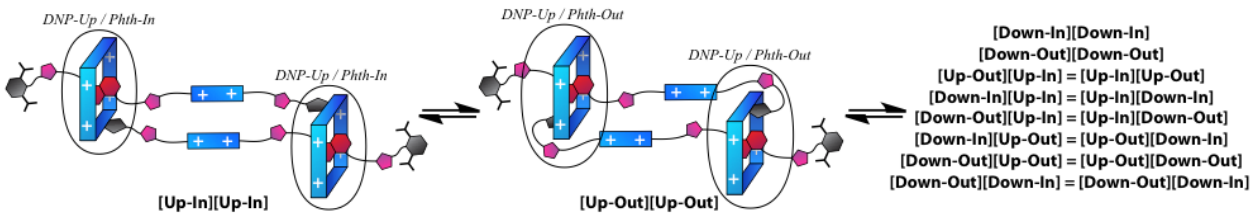


**Scheme S7**. The 10 co-conformational isomers that can be adopted in principle by ***c*2DC$^{12+}$**.

Since the two DNP⊂BB$^{4+}$ subcomplexes are not in close proximity, however, they are unlikely to 'communicate', i.e., the configuration of one complex is unlikely to affect the chemical shifts of protons in the other complex). Assuming this lack of communication between each half of the daisy chain, we can consider only a single DNP⊂BB$^{4+}$ subcomplex, for which we can expect eight H-4/8 DNP proton signals: two from each of the *Up-In*, *Up-Out*, *Down-In*, and *Down-Out* co-conformations of the DNP⊂BB$^{4+}$ subcomplexes, corresponding to the four structures highlighted in Scheme 3 of the main text. Indeed, careful inspection of the H-4/8 DNP proton signals at low temperatures in Figure S9 reveals that all eight doublets are present. We used the line-fitting algorithm in the Mestrenova software suite (Mestrelab Research) to deconvolute the DNP signals to obtain a ratio of 7:14:15:64 for the four isomers (Figure S10) in the ground state distribution.

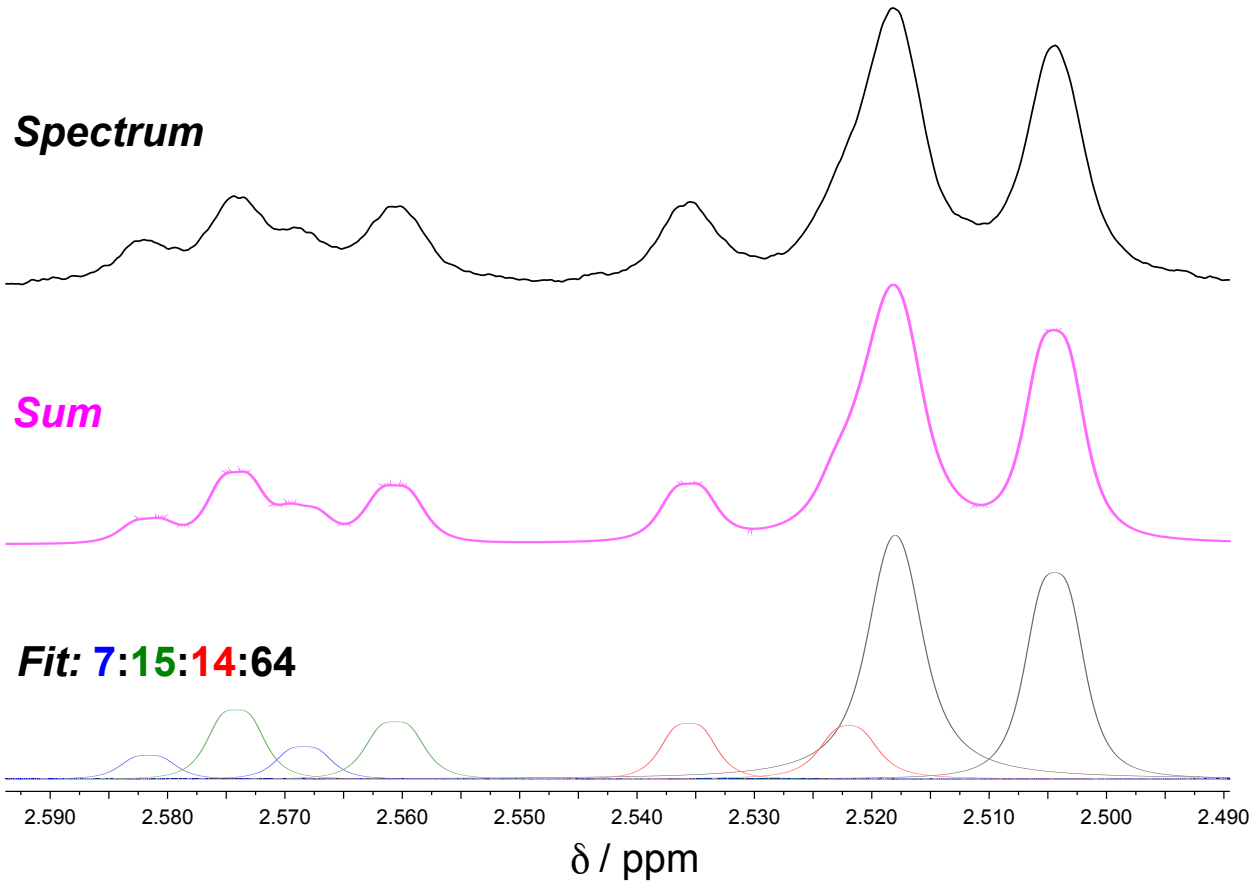


**Figure S10**. Deconvolution of half of the H-4/8 DNP region in the $^{1}$H NMR spectrum of ***c*2DC**·12PF$_6$ (600 MHz, CD$_3$CN) at –10 °C. Integration of the doublets corresponding to all four co-conformations of the DNP⊂BB$^{4+}$ subcomplex (associated with exchange Processes I and II, see Scheme 3 in the main text) allows for quantification of the distribution of co-conformations.

Although ***c*2DC**$^{12+}$ is a mixture of isomers, the dominant co-conformation representing almost two-thirds of the molecular population was fully assigned (Figure S11) and ascribed to the *DNP-Up/Phth-In* co-conformation using the same two-dimensional methods (Figures S12 and S13) as those described in Section 4.2.

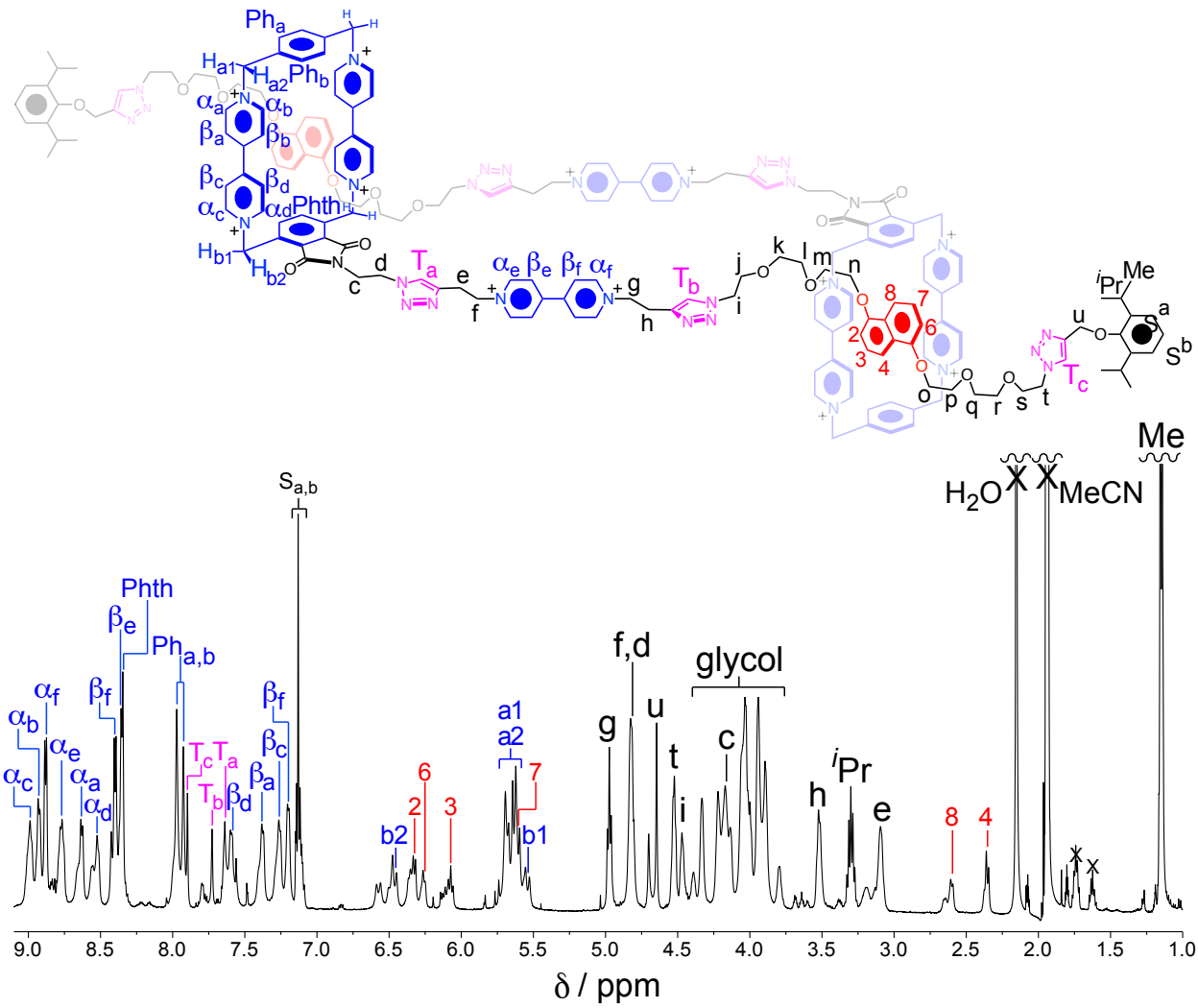


**Figure S11**. $^1$H NMR Spectrum (500 MHz, $CD_3CN$, 298 K) of daisy chain ***c*2DC**·12$PF_6$.

The full VT $^1$H NMR spectrum of ***c*2DC**$^{12+}$ in the range from 80 down to 0 °C is in Figure S14. The spectrum is remarkably similar to that of ***c*1DC**$^{6+}$ at 80 °C, with a single set of signals and significant broadening of several DNP and BB$^{4+}$ resonances which separate out as the temperature is lowered.

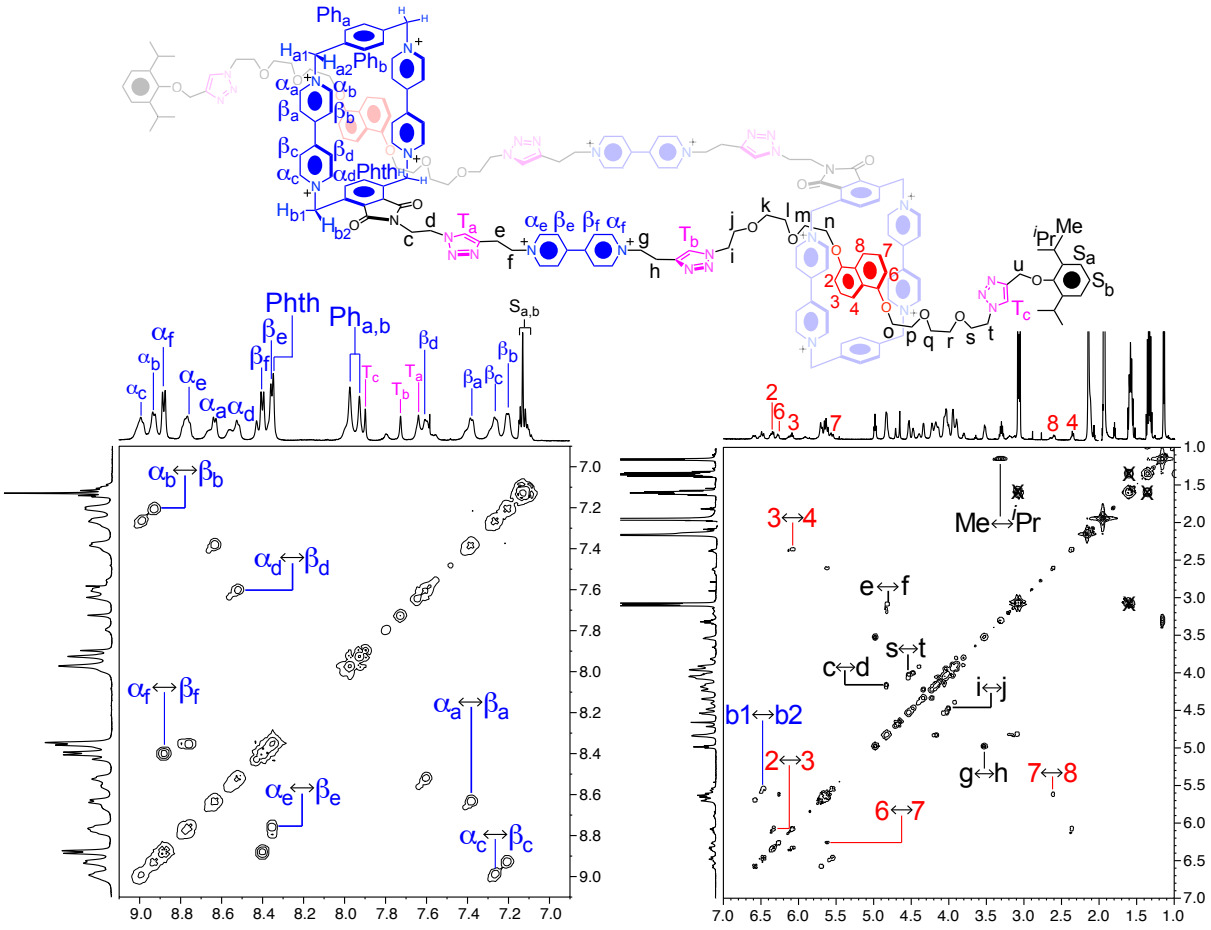

**Figure S12**. $^{1}$H–$^{1}$H gCOSY Spectrum (500 MHz, $CD_3CN$, 298 K) of the daisy chain ***c*2DC**·12$PF_6$

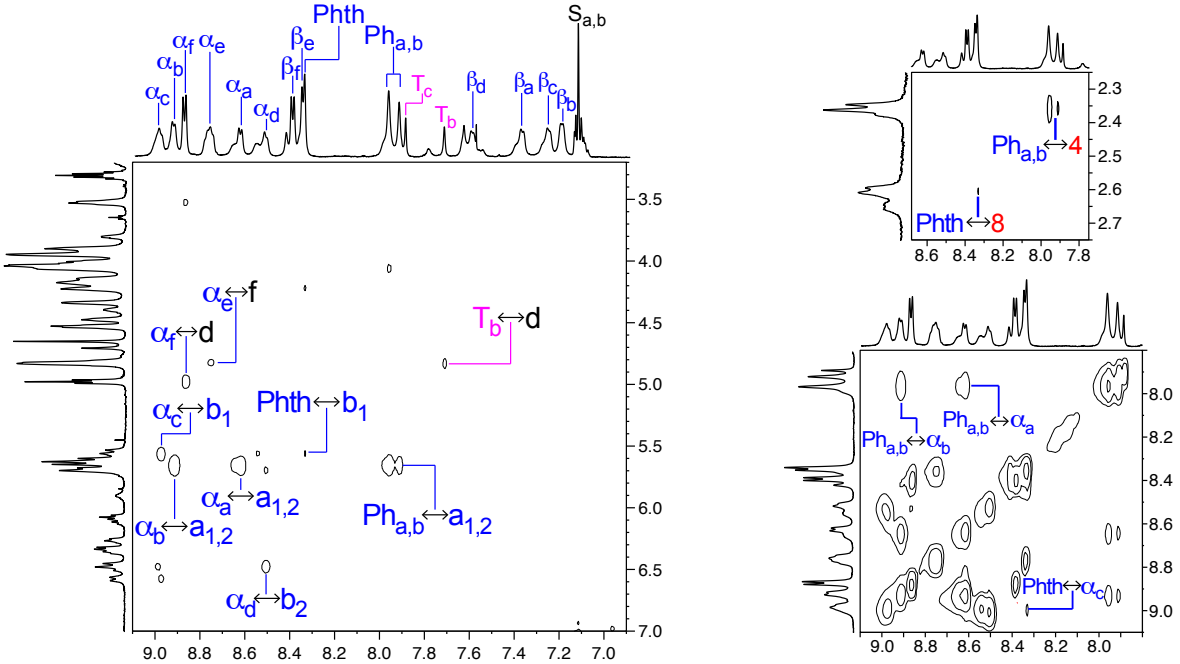

**Figure S13**. $^{1}$H–$^{1}$H gNOESY Spectrum (500 MHz, $CD_3CN$, 298 K) of ***c*2DC**·12$PF_6$

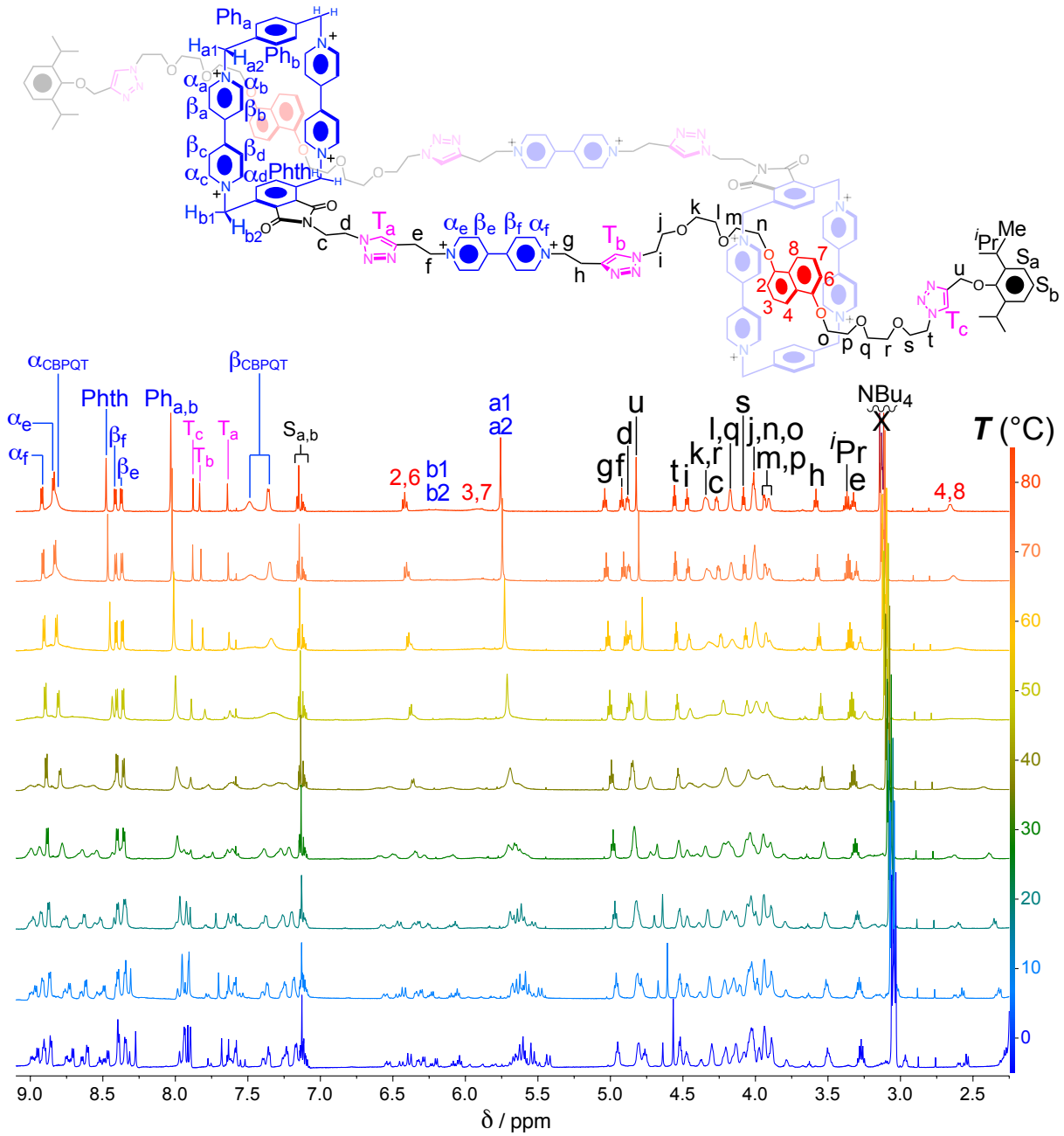


**Figure S14**. VT $^1$H NMR Spectrum (600 MHz, $CD_3CN$) of ***c*2DC**·12$PF_6$

### 4.4. $^1$H NMR Spectroscopic Analysis of [*c*3]Daisy Chain *c*3DC·18$PF_6$

Although the [*c*3]daisy chain was not isolated in sufficient quantity to obtain more than a $^1$H NMR spectrum with acceptable signal-to-noise resolution, the $^1$H NMR spectrum of the ***c*3DC$^{18+}$** is very similar to that of its two-component homologue ***c*2DC$^{12+}$**. Figure S15 illustrates comparisons of the $^1$H NMR spectra of the [*c*2]- and [*c*3]daisy chains at +80 °C (Figure S15a) and +10 °C (Figure S15b). Since the two compounds share all of the same signals with nearly

identical chemical shifts, it stands to reason that the assignments of these signals are also identical. The only apparent difference between the two spectra is in the ratio of *DNP-Up* /*DNP-Down* and *Phth-In/Phth-Out* co-conformations. Whereas a 7:14:15:64 ratio was observed for ***c*2DC**$^{12+}$, there is no indication that any single co-conformation is favored in the case of ***c*3DC**$^{18+}$. Since the [*c*3]daisy chain is the largest and most flexible member of the cyclic homologues, this observation is consistent with the hypothesis that ring strain in the ultramacrocycle can bias the co-conformational ratio.

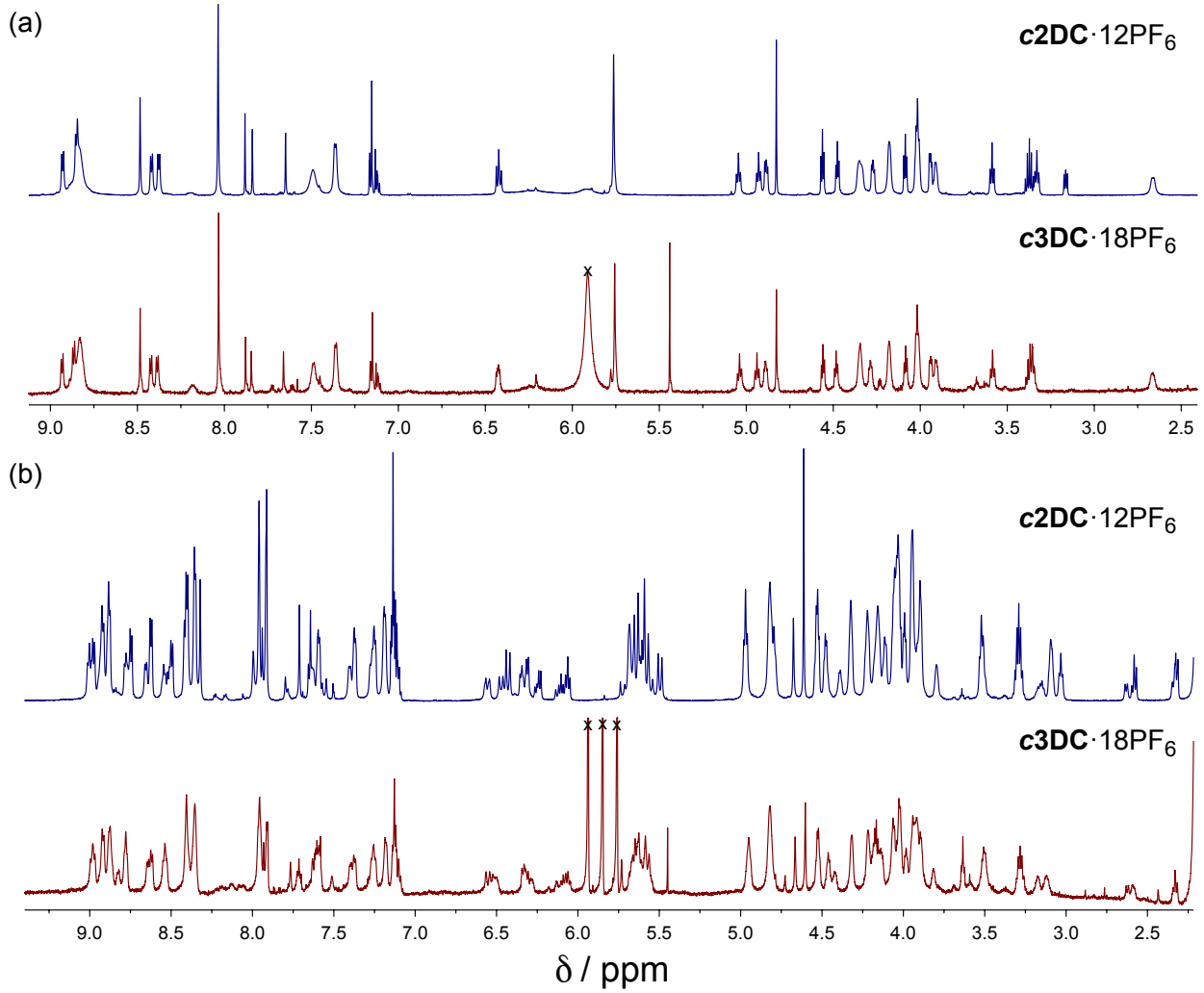


**Figure S15**. A comparison of the $^1$H NMR spectra (600 MHz, $CD_3CN$) of ***c*3DC**·18PF$_6$ (red traces) and ***c*2DC**·12PF$_6$ (blue traces) at (a) +80 °C (fast exchange regime), and (b) +10 °C (slow exchange regime).

The VT $^1$H NMR spectrum of ***c*3DC**$^{18+}$ (Figure S16) is also nearly identical to that (Figure S14) of ***c*2DC**$^{12+}$ especially in the DNP region, so the energy barriers associated with its DNP

molecular dynamics are also similar. The Phth signal, however, coalesces at significantly lower temperatures (+20 °C) in ***c*3DC**$^{18+}$ than in the case of the smaller cyclic counterparts, suggesting that more structural flexibility lowers the activation barrier to the exchange processes occurring in these daisy chains.

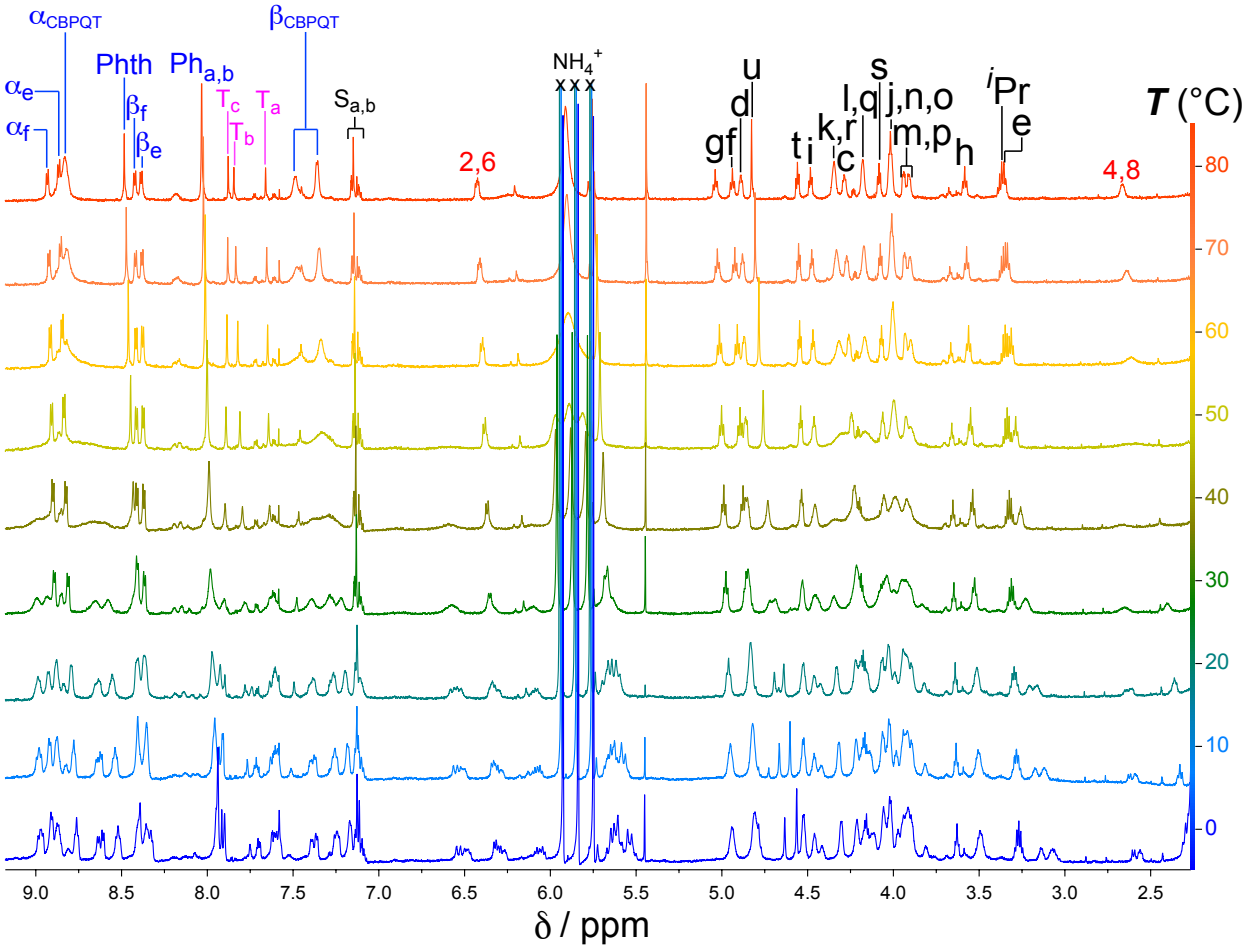


**Figure S16**. VT $^{1}$H NMR spectrum (600 MHz, $CD_3CN$) of ***c*3DC**·18$PF_6$

### 4.5. $^{1}$H NMR Spectroscopic Analysis of [*a*2]Daisy Chain *a*2DC·12$PF_6$

Although ***a*2DC**$^{12+}$ contains significantly more unique protons than its cyclic homologues, all of them experience local environments that are similar to those in either the ***a*1DC**$^{6+}$ monomer or the [*c*2]daisy chain ***c*2DC**$^{12+}$, since both complexed and uncomplexed $BB^{4+}$ and DNP units are represented in ***a*2DC**$^{12+}$. As a result, the $^{1}$H NMR spectrum (Figure S17b) of ***a*2DC**$^{12+}$ is almost the sum of the $^{1}$H NMR spectra of ***a*1DC**$^{6+}$ and ***c*2DC**$^{12+}$, which are shown for comparison in Figures S17a and S17c, respectively. With the aid of this comparison, the aromatic $^{1}$H signals in

the spectrum of ***a*2DC**$^{12+}$ were assigned at +80 °C (Figure S18), where the fast exchange of protons associated with the DNP⊂BB$^{4+}$ 'subcomplex' reduces the number of signals and so facilitates their assignment.

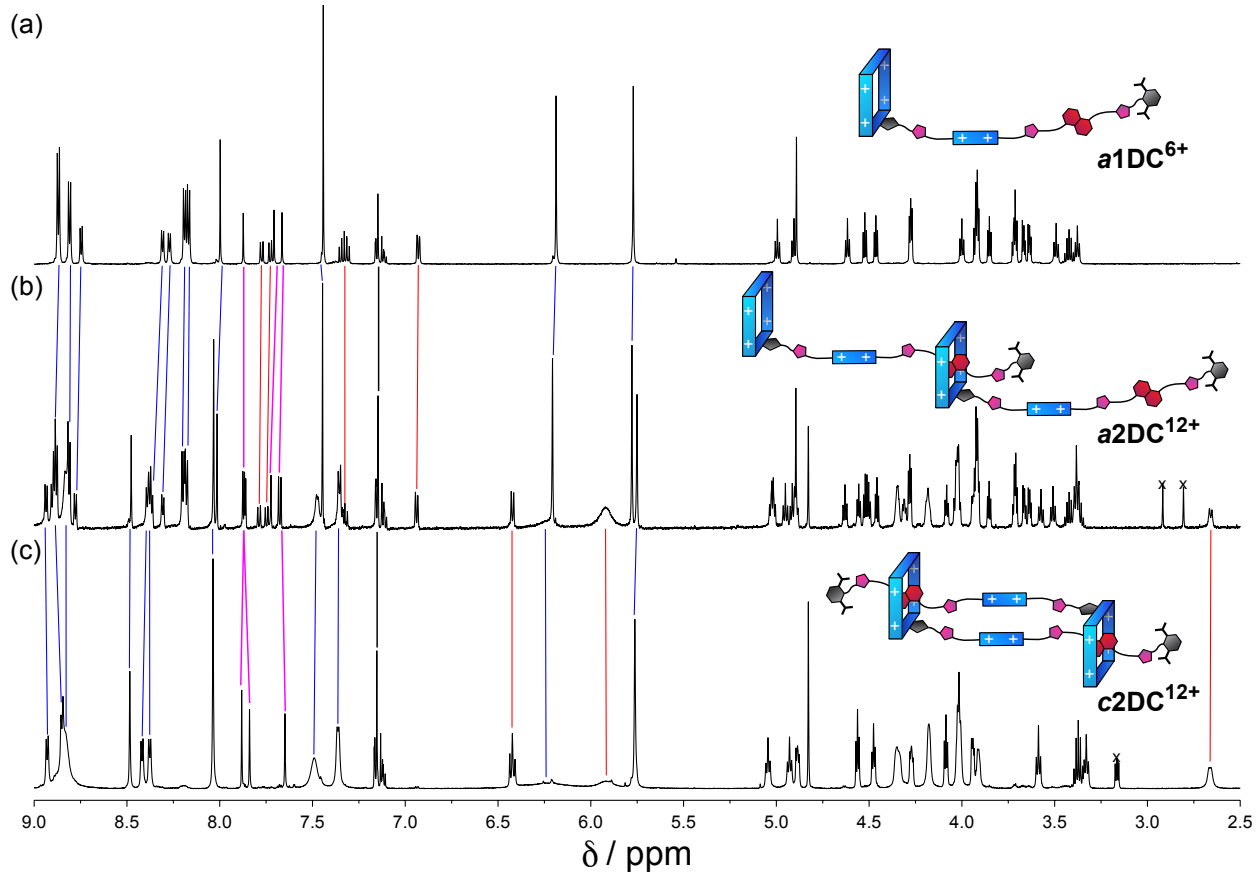


**Figure S17**. Comparison of the $^{1}$H NMR spectra (600 MHz, $CD_3CN$, 353 K) of (a) monomer ***a*1DC**·6$PF_6$, (b) [*a*2]daisy chain ***a*2DC**·12$PF_6$, and (c) [*c*2]daisy chain ***c*2DC**·12$PF_6$.

In the VT $^{1}$H NMR spectrum (Figure S18) of ***a*2DC**$^{12+}$ the H-2/6 and H-4/8 DNP proton signals, which are separated at 0 °C by 30 and 150 Hz respectively, coalesce at approximately 25 and 40 °C, respectively. The ratio of these separate groups of DNP signals at 0 °C is essentially 1:1. This observation is consistent with the hypothesis – discussed in Sections 3.2–3.4 – that ring strain biases the *DNP-Up*:*DNP-Down* ratio in the cyclic daisy chains, since the acyclic compounds have no ultramacrocycle that is capable of experiencing any ring strain. The energy barrier associated with the pirouetting motion of the complexed DNP unit of ***a*2DC**$^{12+}$ is approximately 14.8 kcal·mol$^{-1}$, based on calculated energy barriers of 14.8 and 14.9 kcal·mol$^{-1}$

for the H-4/8 and H-2/6 DNP protons, respectively. These energy barriers are lower than any observed in the case of the cyclic daisy chains. These lower barriers can also be attributed to the greater conformational freedom associated with the less-constrained geometry of the linear daisy chains.

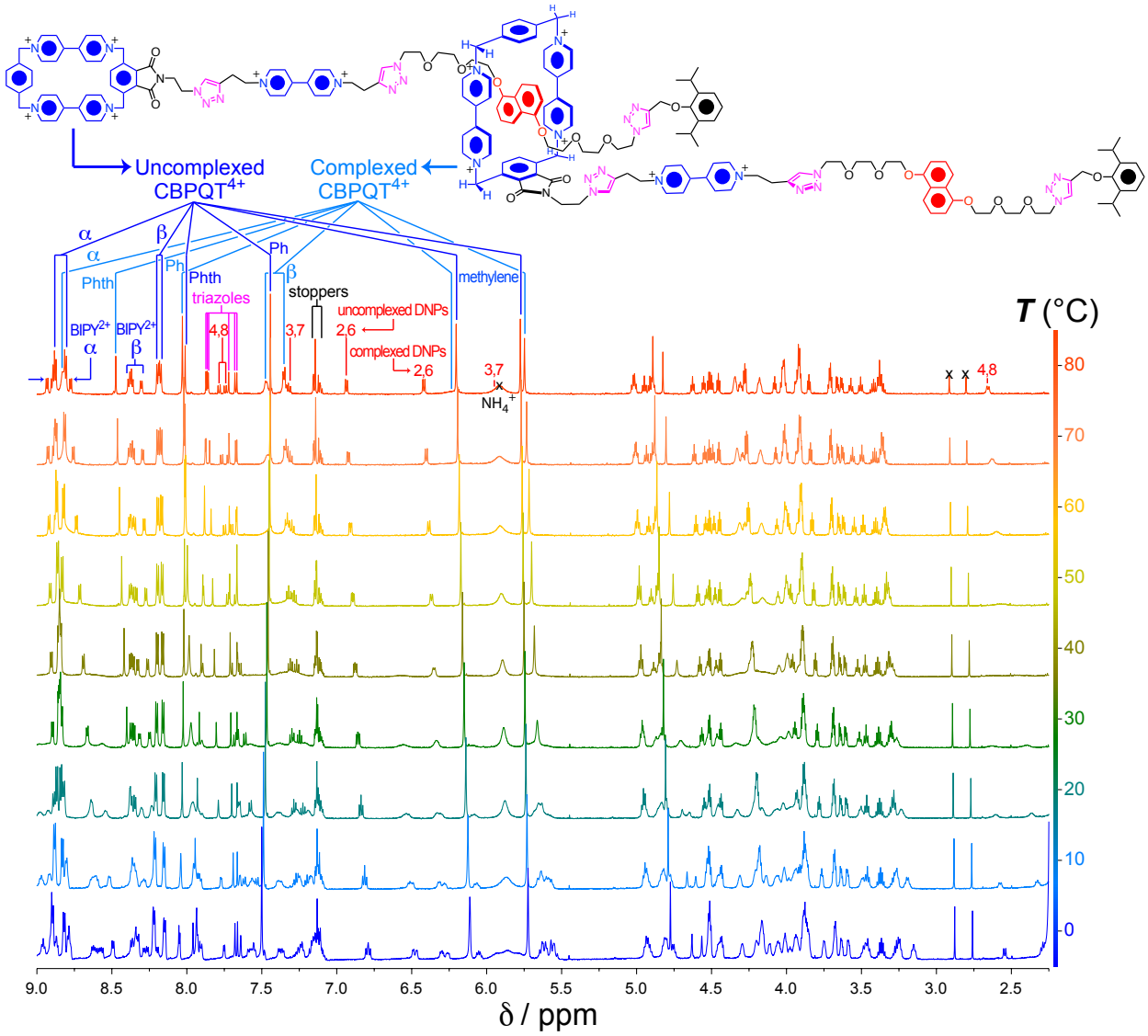


**Figure S18**. VT $^{1}$H NMR spectrum (600 MHz, $CD_3CN$) of ***a*2DC**·12$PF_6$

## 5. Electrochemistry and Spectroelectrochemistry

### 5.1. Characterization of $HV^{\bullet+}\subset BBN_3^{2(\bullet+)}$

We have characterized (Figure S19) the inclusion complex comprising a 1:1 mixture of $\mathbf{HV}^{\bullet+}$ and $\mathbf{BBN_3}^{2(\bullet+)}$ by cyclic voltammetry (CV) and absorption spectroscopy to establish a basis for comparison with the daisy chain assemblies.

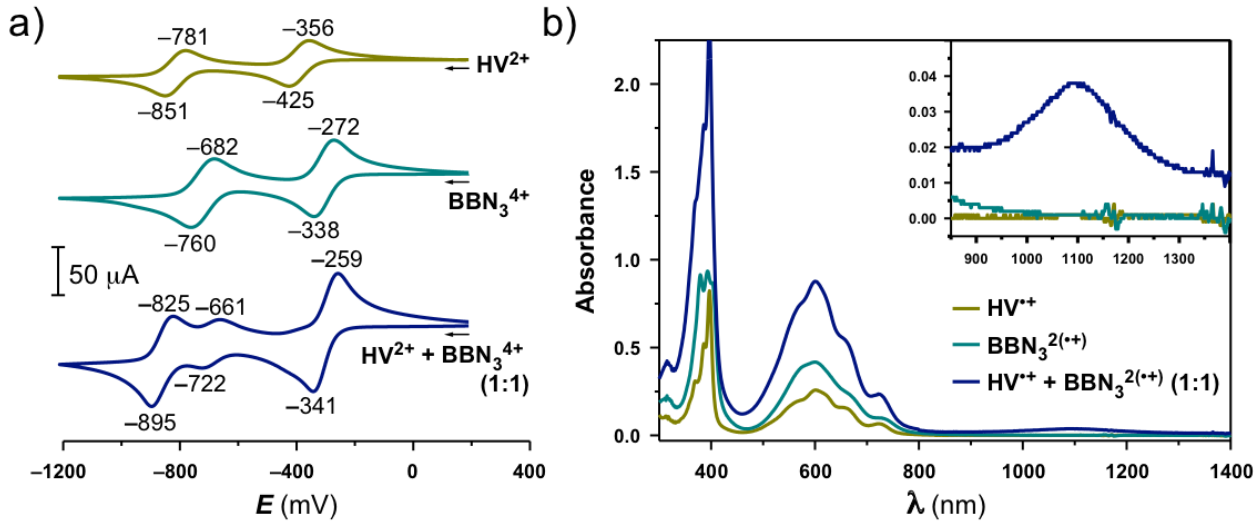


**Figure S19.** Electrochemical and spectroelectrochemical characterization of the $\mathbf{HV^{\bullet+}\subset BBN_3^{2(\bullet+)}}$ inclusion complex. (a) The CV of a 1:1 mixture of $\mathbf{HV}\cdot 2PF_6$ and $\mathbf{BBN_3}\cdot 4PF_6$ at 1 mM in MeCN ( 0.1 M $NBu_4PF_6$, 298 K, 100 $mV\cdot s^{-1}$). (b) Visible/Near-IR absorption profile of a 1:1 mixture of $\mathbf{HV^{\bullet+}}$ and $\mathbf{BBN_3^{2(\bullet+)}}$ at 20 μM in MeCN (0.1 M $NBu_4PF_6$, 298 K) at an applied voltage of –0.55 V, compared with isolated $\mathbf{HV^{\bullet+}}$ and $\mathbf{BBN_3^{2(\bullet+)}}$ samples under the same conditions. The inset reveals an expansion of the near-IR region showing a very weakly absorbing broad band near λ = 1100 nm.

The CV of a 1:1 mixture of $\mathbf{HV^{2+}}$ and $\mathbf{BBN_3^{4+}}$, each at a concentration 1 mM in MeCN, is compared with that of the corresponding isolated components in Figure S19a. Evidence for the formation of a $\mathbf{HV^{\bullet+}\subset BBN_3^{2(\bullet+)}}$ complex at this concentration is provided primarily by the 1:2 integration of the final two redox waves at –692 and –860 mV, an observation which is indicative of a one-electron process involving the less interactive unpaired $BIPY^{\bullet+}$ radical cation of the cyclophane in the $\mathbf{HV^{\bullet+}\subset BBN_3^{2(\bullet+)}}$ complex, and a two-electron process involving the neutralization/reoxidation of a $\mathbf{HV^{\bullet+}\subset BBN_3^{\bullet+}}$ complex, stabilized by favorable radical pairing interactions, respectively. The negative shift in this final redox process is modest, however, compared to the daisy chains – see Figures 5–6 and the corresponding discussion in the main text – indicating that the $\mathbf{HV^{\bullet+}\subset BBN_3^{2(\bullet+)}}$ radicals are more weakly associated. The same complex at 20 μM in MeCN at an applied potential of –550 mV can scarcely be detected by absorption spectroscopy. The visible/near-IR absorption spectrum (Figure S19b) of the 1:1 $\mathbf{HV^{\bullet+}:BBN_3^{2(\bullet+)}}$ mixture is essentially a sum of the $\mathbf{HV^{\bullet+}}$ and $\mathbf{BBN_3^{2(\bullet+)}}$ spectra under the same conditions, with the exception of a very low-intensity absorption band centered near 1100 nm (inset in Figure S19b) which suggests that the inclusion complex is not completely absent.

### 5.2. Characterization of $BBV^{3(\bullet+)}$

The electrochemical characterization of the blue box–viologen monomer $\mathbf{BBV}^{6+}$ is summarized in Figure S20. The irreversible process associated with the first reduction of $\mathbf{BBV}^{6+}$ was probed (Figure S20a) by variable scan-rate CV. All of the redox processes in the cathodic window of the CV exhibit minimal changes across a wide range of scan rates, with the exception of the final re-oxidation process in the return scan. At a scan-rate of 10 $mV \cdot s^{-1}$, the redox couple associated with $\mathbf{BBV}^{6+} \leftrightarrow \mathbf{BBV}^{3(\bullet+)}$ centered at approximately –260 mV is nearly reversible, with only a small shoulder peak that is shifted to a more positive potential. This additional peak becomes increasingly intense and more positively shifted with increasing scan-rates, reaching a potential of +15 mV at 1500 $mV \cdot s^{-1}$. This behavior is indicative of a dynamic process, which influences the oxidation potential of the $V^{\bullet+}$ radical cation, occurring on roughly the same timescale as that of the CV scan. We propose that steric constraints associated with the relatively short covalent linkage between viologen and blue box raise the energy barrier for dissociation of the transient $V^{\bullet+} \subset BB^{(2+)(\bullet+)}$ complex enough to push its kinetics below the timescale of the CV scan at faster scan-rates. The electrochemical behavior of $BBV^{6+}$ and, particularly, the positive shift in the redox potential is similar to that observed previously[S9] for $V^{\bullet+} \subset BB^{2(\bullet+)}$ radicals stabilized in rotaxanes which utilize the sterics of mechanical bonds to constrain the viologen and blue box components into very close proximity.

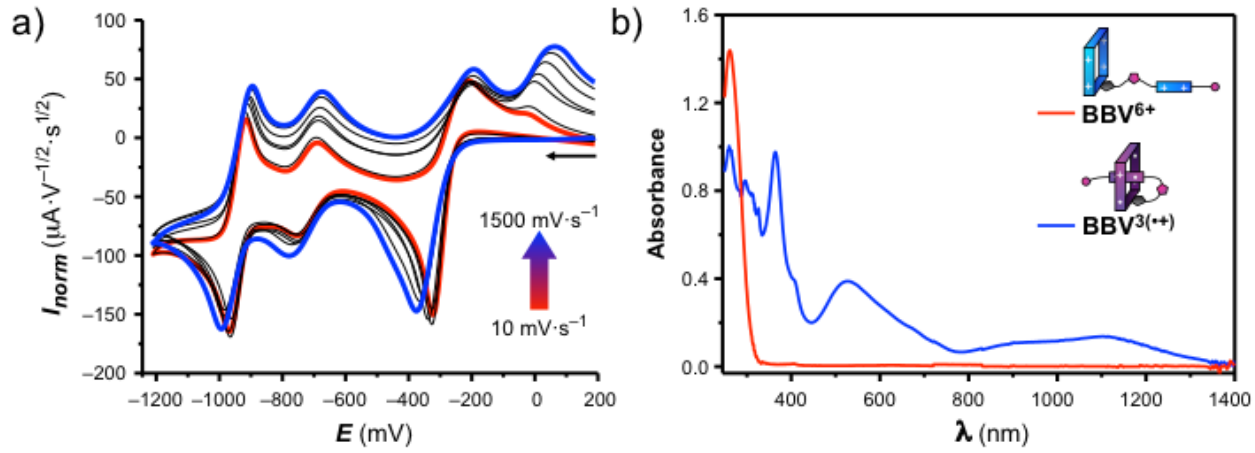


**Figure S20**. Electrochemical characterization of $\mathbf{BBV} \cdot 6PF_6$. (a) Variable scan-rate cyclic voltammogram of $\mathbf{BBV} \cdot 6PF_6$. (b) Comparison of the visible/near-IR absorption profile of the blue box–viologen monomer at applied potentials of 0 mV ($\mathbf{BBV}^{6+}$, red curve) and –550 mV ($\mathbf{BBV}^{3(\bullet+)}$, blue curve) at a concentration of 20 μM in MeCN (0.1 M $NBu_4PF_6$, 298 K).

The absorption profiles of the $\mathbf{BBV}^{6+}$ monomer and the $\mathbf{BBV}^{3(\bullet+)}$ trisradical complex are compared in Figure S20b. This comparison shows that any absorption bands at wavelengths >350 nm must be attributed to bipyridinium radical cations, since $\mathbf{BBV}^{6+}$ does not absorb light in the visible region of the spectrum. The spectrophotometric data in Figure S21 verify that the inclusion complex in $\mathbf{BBV}^{3(\bullet+)}$ undergoes an 'ouroboros' [*c*1]daisy chain assembly. The comparison between the absorption spectra of a 1:1 $\mathbf{HV}^{\bullet+}$:$\mathbf{BBN_3}^{2(\bullet+)}$ mixture and $\mathbf{BBV}^{3(\bullet+)}$ at 20 μM in MeCN (Figure S21a) shows that $\mathbf{BBV}^{3(\bullet+)}$ absorbs differently than the dilute 1:1 $\mathbf{HV}^{\bullet+}$:$\mathbf{BBN_3}^{2(\bullet+)}$ mixture – which was found to be all but dissociated under these conditions in Section 5.1 – with intense absorption bands at 364 and 526 nm and weaker broad absorption bands at 885 and 1115 nm that confirm the presence of a $V^{\bullet+}\subset BB^{2(\bullet+)}$ inclusion complex in $\mathbf{BBV}^{3(\bullet+)}$. From this comparison, it is evident that the covalent linkage between the viologen and blue box moieties of $\mathbf{BBV}^{6+}$ enhances their tendency to interact and form a $V^{\bullet+}\subset BB^{2(\bullet+)}$ complex under reductive conditions. Although this comparison already points to a strong unimolecular complexation, it was further verified by observing (Figure S21b) the invariant extinction coefficient of $\mathbf{BBV}^{3(\bullet+)}$ from 1–100 μM.

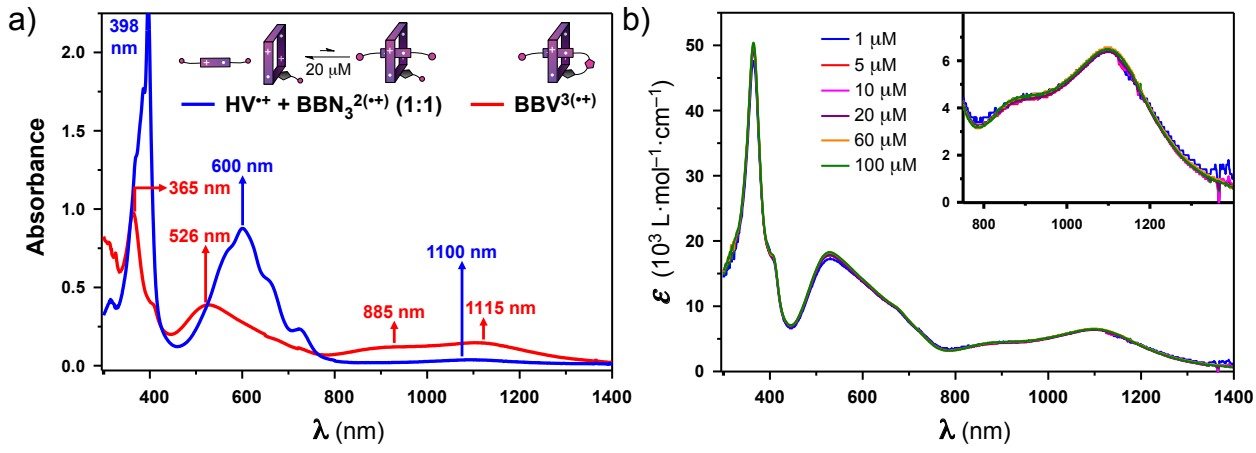


**Figure S21**. Verification of the unimolecular nature of the trisradical inclusion complex in $\mathbf{BBV}^{3(\bullet+)}$ by spectroelectrochemistry (–550 mV, MeCN, 0.1 M $NBu_4PF_6$, 298 K). (a) Comparison of the absorption profiles of 1:1 $\mathbf{HV}^{\bullet+}$:$\mathbf{BBN_3}^{2(\bullet+)}$ (blue curve) and $\mathbf{BBV}^{3(\bullet+)}$ (red curve) at a concentration of 20 μM. (b) The extinction coefficient of $\mathbf{BBV}^{3(\bullet+)}$ plotted against wavelength, which remains constant over the range of 1 μM–100 μM. The inset is an expansion of the near-IR region of the spectrum.

### 5.3. Characterization of the Molecular Daisy Chains

The differentiation of two peaks in the irreversible process associated with the re-oxidation of the $V^{\bullet+}\subset BB^{2(\bullet+)}$ complex in $\mathbf{BBV}^{3(\bullet+)}$, which we attribute to a stabilization of the transient $V^{\bullet+}\subset BB^{(2+)(\bullet+)}$ complex by the short covalent linkage of the ouroboros, is replicated as expected in the CV (Figure S22a) of $\boldsymbol{c}\mathbf{1DC}^{6+}$. At low scan rates, the first redox couple of $\boldsymbol{c}\mathbf{1DC}^{6+}$ is all but reversible, whereas a second peak in the return scan becomes more intense and positively-shifted with increasing scan rates, reaching a potential of +35 mV at 1500 $mV{\cdot}s^{-1}$. By contrast, the CV (Figure S22b) of $\mathbf{c2DC}^{12+}$ is relatively invariant over a range of 10–1500 $mV{\cdot}s^{-1}$, further supporting the argument that steric constrains akin to ring strain in the tightly self-complexed momomers $\mathbf{BBV}^{3(\bullet+)}$ and $\boldsymbol{c}\mathbf{1DC}^{3(\bullet+)}$ are responsible for the irreversibility of the redox processes in the case of the latter, since the dimerized monomers in $\boldsymbol{c}\mathbf{2DC}^{12+}$ render a much more flexible ultramacrocycle. A subtle positively-shifted shoulder peak appears, however, at 1500 $mV{\cdot}s^{-1}$ in the CV of $\boldsymbol{c}\mathbf{2DC}^{12+}$, indicating a much lower energy barrier to the same process described for the [*c*1] assemblies.

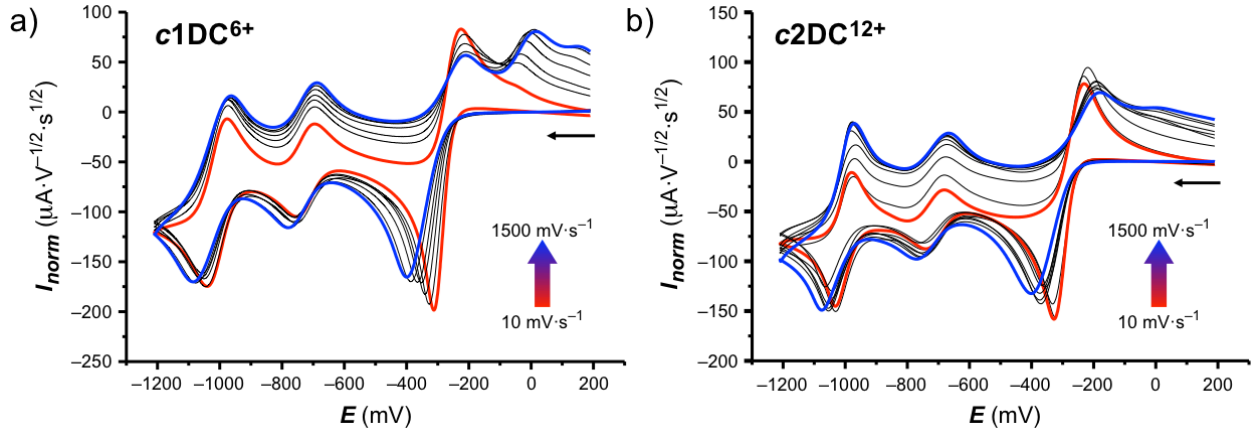


**Figure S22**. Variable scan-rate CVs of the cyclic daisy chains (a) $\boldsymbol{c}\mathbf{1DC}{\cdot}6PF_6$ and (b) $\boldsymbol{c}\mathbf{2DC}{\cdot}12PF_6$ at a concentration of 1 mM in MeCN (0.1 M $NBu_4PF_6$, 298 K).

The visible/near-IR absorption profiles of the monomeric and dimeric molecular daisy chain assemblies are compared in the ground state co-conformation (0 mV) and radical state co-conformation (–550 mV) in MeCN in Figure S23. See the main text for a discussion of these absorption profiles.

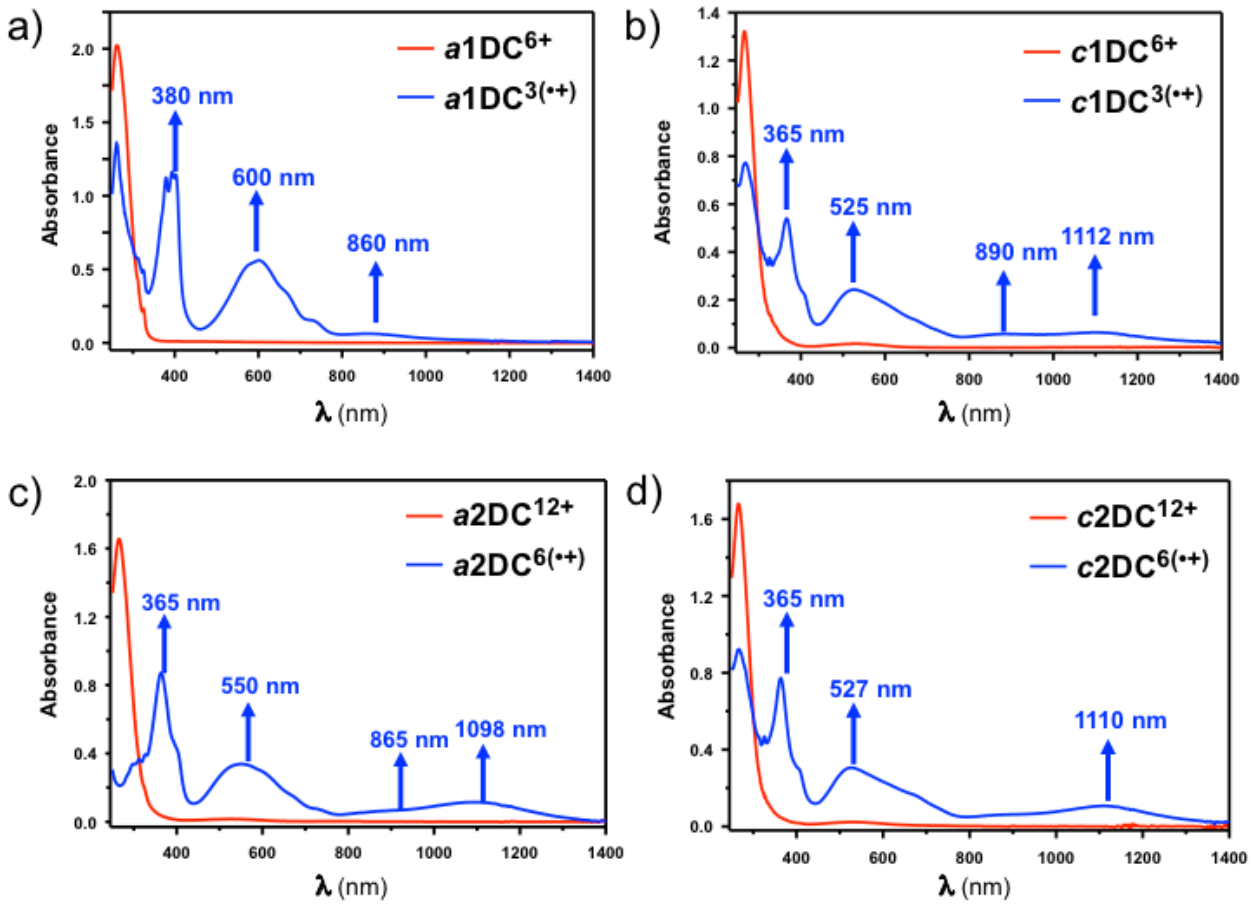


**Figure S23**. Comparison of the visible/near-IR absorption profiles (20 μM, MeCN, 0.1 M $NBu_4PF_6$, 298 K) of the monomeric and dimeric daisy chains at applied voltages of 0 mV (red curves) and –550 mV (blue curves): (a) ***a*1DC**·$6PF_6$; (b) ***c*1DC**·$6PF_6$; (c) ***a*2DC**·$12PF_6$; (d) ***c*2DC**·$12PF_6$.

## 6. References


(S1) Ishii, H.; Harada, Y.; Asaka, T.; Murakami, Y.; Honaoka, T.; Ikeda, N. *Yakugaku Zasshi* **1976**, *96*, 1259–1264.

(S2) Zhu, Z.; Li, H.; Liu, Z.; Lei, J.; Zhang, H.; Botros, Y. Y.; Stern, C. L.; Sarjeant, A. A.; Stoddart, J. F.; Colquhoun, H. M. *Angew. Chem., Int. Ed.* **2012**, *51*, 7231–7235.

(S3) Amabilino, D. B.; Anelli, P.-L.; Ashton, P. R.; Brown, G. R.; Córdova, E.; Godínez, L.; Hayes, W.; Kaifer, A. E.; Philp, D.; Slawin, A. M. Z.; Spencer, N.; Stoddart, J. F.; Tolley, M. S.; Williams, D. J. *J. Am. Chem. Soc.* **1995**, *117*, 11142–11170.

(S4) Dichtel, W. R.; Miljanić, O. Š.; Spruell, J. M.; Heath, J. R.; Stoddart, J. F. *J. Am. Chem. Soc.* **2006**, *128*, 10388–10390.

(S5) Coskun, A.; Saha, S.; Aprahamian, I.; Stoddart, J. F. *Org. Lett.* **2008**, *10*, 3187–3190.

(S6) Li, H.; Zhao, Y.-L.; Fahrenbach, A. C.; Kim, S.-Y.; Paxton, W. F.; Stoddart, J. F. *Org. Biomol. Chem.* **2011**, *9*, 2240–2250.

(S7) Amabilino, D. B.; Anelli, P.-L.; Ashton, P. R.; Brown, G. R.; Córdova, E.; Godínez, L.; Hayes, W.; Kaifer, A. E.; Philp, D.; Slawin, A. M. Z.; Spencer, N.; Stoddart, J. F.; Tolley, M. S.; Williams, D. J. *J. Am. Chem. Soc.* **1995**, *117*, 11142–11170.

(S8) Zhu, Z.; Bruns, C. J.; Li, H.; Lei, J.; Ke, C.; Liu, Z.; Shafaie, S.; Colquhoun, H. M.; Stoddart, J. F. *Chem. Sci.* **2013**, 4, 1470–1483.

(S9) Li, H.; Zhu, Z.; Fahrenbach, A. C.; Savoie, B. M.; Ke, C.; Barnes, J. C.; Lei, J.; Zhao, Y.-L.; Lilley, L. M.; Marks, T. J.; Ratner, M. A.; Stoddart, J. F. *J. Am. Chem. Soc.* **2013**, *135*, 456–467.